eLife

Reviewed Preprint
v1 • September 9, 2026
Not revised

For correspondence:
vdzhala@mhg.harvard.edu
Staley.Kevin@mgh.harvard.edu

Competing interests: No competing interests declared

Funding: See page 22

Reviewing editor: Patrick Alexander Forcelli, Georgetown University, United States

WNK-SPAK/OSR1 signaling pathway facilitates ictal activity via reduced neuronal chloride extrusion rate

Volodymyr I Dzhala[1], Fu Hung Shiu[1], Negah Rahmati[1], Aloe Carroll[1], Reagan Bae[1], Kristopher T Kahle[2], Kevin J Staley[1]

[1]Department of Neurology, Harvard Medical School and Massachusetts General Hospital, Boston, United States • [2]Department of Neurosurgery, Harvard Medical School and Massachusetts General Hospital, Boston, United States

eLife Assessment

This study presents a **valuable** investigation of how inhibition of the WNK-SPAK/OSR1 pathway influences neuronal chloride homeostasis and seizure-like activity in organotypic hippocampal slice cultures. The evidence supporting the principal mechanistic conclusions is **incomplete** because several proposed mechanisms are inferred from changes in chloride dynamics rather than directly demonstrated. The work will be of interest to researchers studying chloride homeostasis, inhibitory neurotransmission, and epilepsy.

https://doi.org/10.7554/eLife.112181.1.sa3

Abstract

Seizures upregulate Na^+-K^+-$2Cl^-$ (NKCC1)-mediated Cl^- influx and downregulate K^+-Cl^-(KCC2)-mediated Cl^- efflux *via* the WNK-SPAK/OSR1 kinases, leading to cytoplasmic chloride ($[Cl^-]_i$) accumulation, reduced GABAergic inhibition and anticonvulsant failure. Early studies found that inhibiting WNK-kinase reduced baseline $[Cl^-]_i$ (E_{Cl}) and seizures via increased KCC2 activity. However, increased KCC2 activity alone should not affect E_{Cl} whose determinants are more complex. We determined the net effects of WNK-SPAK/OSR1 pathway inhibitor WNK463 on E_{Cl} and $[Cl^-]_i$ transients during spontaneous ictal-like discharges (ILDs). We found that WNK463 reduced interictal $[Cl^-]_i$ but did not change baseline $[Cl^-]_i$ measured in the presence of TTX. WNK463 enhanced neuronal Cl^- extrusion during and after ILDs, before abolishing ILDs. Pharmacological inhibition and targeted siRNA silencing demonstrated that the anti-ictal effects of WNK463 involved both NKCC1 and KCC2. Thus, mutual NKCC1 inhibition and KCC2 activation via the WNK-SPAK/OSR1 pathway exert powerful anti-ictal effects by facilitating $[Cl^-]_i$ extrusion during ILDs.

Introduction

Acute brain injury is often complicated by anticonvulsant (AED) resistant seizures (Liesemer et al., 2011). One potential mechanism of these seizures and AED failure is the inversion of signaling by the inhibitory neurotransmitter GABA in injured neurons. Acute brain injury results in cytotoxic cerebral edema, i.e., an influx of NaCl into neurons and glia (Van Harreveld and Schade, 1959;Steffensen et al., 2015). This NaCl influx results in an elevated baseline $[Cl^-]_i$ and a consequent depolarizing shift in the reversal potential for $GABA_A$ receptor-mediated currents (E_{GABA}) (van den Pol et al., 1996;Pond et al., 2006;Dzhala et al., 2012;Kahle et al., 2008;Blaesse et al., 2009). Depolarizing GABA responses facilitate neuronal network activity and contribute to initiation of seizures (Dzhala and Staley, 2003;Khazipov et al., 2004). Furthermore high rates of synaptic Cl^- influx during seizures stress neuronal Cl^- homeostasis (Staley and Proctor, 1999) and shift E_{GABA} to more positive potentials, contributing to prolonged seizures and anticonvulsant-resistance (Khalilov et al., 2003;Dzhala et al., 2010).

After synaptically-mediated Cl^- influx, restoration of $[Cl^-]_i$ equilibrium is achieved by the activities of the cation-Cl^- co-transporters (CCCs) such as the Na^+-driven NKCC1, which is biased toward Cl^- influx, and the K^+-driven KCC2, which is biased toward Cl^- efflux (Staley, 2024). Depending on the ionic and osmotic gradients across the neuronal cytoplasmic membrane, either antagonizing or stimulating CCCs activity may be a useful therapeutic strategy to reduce $[Cl^-]_i$ accumulation, restore GABAergic inhibition, and suppress seizures (Glykys et al., 2017). Previous studies have demonstrated that inhibition of NKCC1 reduced $[Cl^-]_i$ in injured neurons, enhanced GABAergic inhibition and the efficacy of anticonvulsants (Pond et al., 2006;Dzhala et al., 2008;Dzhala et al., 2024;Nardou et al., 2011;Cleary et al., 2013;Sivakumaran and Maguire, 2016; Soul et al., 2021). Conversely, enhancement of KCC2 activity improved $[Cl^-]_i$ extrusion and control of seizures (Gagnon et al., 2013;Moore et al., 2018;Dzhala and Staley, 2021).

Transmembrane Cl^- equilibrium is mediated by a Donnan mechanism that involves intra- and extracellular impermeant anions, in which the CCCs comprise the requisite cation-chloride membrane permeability (Glykys et al., 2017;Bahari et al., 2024). Increasing cation-chloride permeability by increasing the maximum velocity of CCCs should not change the baseline $[Cl^-]_i$. However, in injured neurons with elevated $[Cl^-]_i$, increased cation-chloride extrusion might reduce neuronal volume and $[Cl^-]_i$. Further, increasing the maximum velocity of CCCs should increase the ability of neurons to buffer large ictal synaptically-mediated Cl^- influxes. The maximum velocity of CCCs is regulated by the WNK-SPAK/OSR1 kinase pathways (Kahle et al., 2006;Melo et al., 2013;Alessi et al., 2014). In hypertonic extracellular conditions, WNK-SPAK/OSR1 signaling phosphorylates NKCC1 (Moriguchi et al., 2005;Vitari et al., 2006), rapidly enhancing its activity and chloride uptake (Côme et al., 2023). In isotonic conditions KCC2 is phosphorylated and inactive, whereas hypotonic conditions promote dephosphorylation and activation of KCC2 (Kahle et al., 2013;Pisella et al., 2019;Watanabe et al., 2019). Therefore, blocking the phosphorylation of KCC2 and NKCC1 via WNK signaling would shift net membrane transport toward maximum Cl^- extrusion, preventing excessive $[Cl^-]_i$ accumulation in conditions such as traumatic brain injury and seizures.

The recently identified WNK-kinase inhibitor WNK463 reduces phosphorylation of downstream targets SPAK/OSR1 (Yamada et al., 2017) and thereby inhibits NKCC1 and KCC2 phosphorylation (de Los et al., 2014), resulting in reciprocal inhibition of NKCC1 and stimulation of KCC2 activity. WNK463 reduced KCC2-Thr1007 phosphorylation, hyperpolarized E_{GABA} and limited status epilepticus (Lee et al., 2022). The relative contribution of the WNK-SPAK/OSR1 pathway in the net regulation of the NKCC1 and KCC2 transport activity (velocity) and $[Cl^-]_i$ transients during recurrent seizures was not determined. We determine now the net effects of WNK-SPAK/OSR1 pathway inhibitor WNK463 on $[Cl^-]_i$ elevation and extrusion rates during spontaneous ILDs, and the correlation between ionic and electrographic effects in an *in vitro* model of post-traumatic epilepsy.

Results

Chloride transients during recurrent ILDs

Organotypic hippocampal slices from mice expressing the genetically encoded intracellular chloride fluorophore Clomeleon or Super Clomeleon (Grimley et al., 2013) were used as a model of acute traumatic brain injury and epileptogenesis *in vitro* (Dyhrfjeld-Johnsen et al., 2010;Berdichevsky et al., 2012;Dzhala et al., 2012). Simultaneous extracellular field potential recordings and two-photon imaging were performed in the CA1 pyramidal cell layer to monitor neuronal network activity and $[Cl^-]_i$ in individual cells (Figure 1). Spontaneous neuronal network activity was characterized by brief interictal-like discharges (IEDs) and prolonged ictal-like discharges (ILDs) reminiscent of seizure-like activity *in vivo*. In control, during the inter-ictal phase between ILDs, the baseline $[Cl^-]_i$ in individual pyramidal cells varied from 5 to 30 mM and higher (Figure 1a). In line with previous studies (Lillis et al., 2012;Glykys et al., 2014), $[Cl^-]_i$ rapidly increased at the onset of ILDs and during sustained high-frequency ictal-tonic discharges (Figure 1b). Elevated $[Cl^-]_i$ levels often persisted during intermittent ictal-clonic

discharges and progressively decreased during secondary after-discharges and termination of ILDs. Postictally, $[Cl^-]_i$ decayed monoexponentially with a decay time constant that varied from 20 to 240 s (Figures 1, 5).

Progressive $[Cl^-]_i$ elevations during the onset of ILDs due to intensive GABAergic inputs in the pyramidal cells may shift the effects of post-synaptic $GABA_A$ receptor ($GABA_A$-R) mediated currents from depolarizing to excitatory and/or reverse the net effects of GABA from inhibitory to excitatory (Lillis et al., 2012; Jedlicka et al., 2011). Such changes may shift a neuronal network into a periodic bursting mode associated with sustained ictal-like discharges and intermittent after-discharges (Figure 1). Therefore, prevention of $[Cl^-]_i$ elevations and/or facilitation of $[Cl^-]_i$ extrusion may improve chloride homeostasis, GABAergic inhibition, and control of electrographic seizures.

The WNK-SPAK/OSR1 inhibitor WNK463 enhanced neuronal chloride extrusion

The Cl^--sensitive WNK-SPAK/OSR1-CCCs pathway, involving WNK (with no lysine or lysine-deficient protein kinase) and downstream SPAK (SPS1-related proline/alanine-rich kinase) and OSR1 (oxidative stress-responsive kinase-1) complex, and cation-chloride cotransporters, regulates cell volume, neuronal chloride homeostasis and corresponding $GABA_A$ signaling (Shekarabi et al., 2017). We determined the role of WNK-SPAK/OSR1 kinase activity in modulation of $[Cl^-]_i$ transients induced by intensive $GABA_A$-R activation in principal neurons. A puff micropipette filled with extracellular solution containing GABA (50 µM) to activate $GABA_A$-Rs and L-Glutamate (50 µM) to depolarize the membrane potential and maximize $GABA_A$-R mediated Cl^- influx was placed above the dendritic area of the neurons. Focal puff application of GABA/L-Glu (puff duration 5-10 ms, pressure 5-10 psi) in ACSF containing TTX (1 µM) induced $[Cl^-]_i$ transients in a subpopulation of superficial neurons (Figure 2a). The decay time constant of baseline $[Cl^-]_i$ recovery was plotted as a function of baseline $[Cl^-]_i$. Linear regression analysis suggested a minimal interaction between baseline $[Cl^-]_i$ and the rate of $[Cl^-]_i$ recovery in individual cells that responded to GABA/L-Glu puff applications (Figure 2b; y=A+B*x, A=57.97±19.4, B=-0.26±0.87; n=6 slices, 17 cells; Pearson's r=-0.078, R^2=0.006).

The decay time constant of $[Cl^-]_i$ recovery in individual cells was compared in control conditions, before and during application of the WNK-SPAK/OSR1 inhibitor WNK463 (1 µM), and the KCC2 inhibitor VU04663271 (1 µM) (Figure 2c-h). To facilitate comparisons between neurons, the chloride transients in cells that responded to GABA/L-Glu puff applications were normalized to values between 0 and 1. Under control conditions, the mean decay time constant of $[Cl^-]_i$ recovery (extrusion) was not significantly different between two consecutive (10-15 min interval) chloride transients (Figure 2c, d; n=5 slices at DIV9-14, 9 cells; 41.73±14.65 compared to 42.54±14.75 s; paired t-test, t=-0.4, P=0.69). Thus, individual neurons within the same slice showed reproducible responses to repeated GABA/L-Glu puffs. However, the variance of responses between slices was much larger, reflecting the variable geometry of the puffer pipette to the dendritic glutamate and $GABA_A$ receptors.

In line with previous studies (Dzhala and Staley, 2021), bath application of the KCC2 inhibitor VU0463271 (1 µM for 10-15 min) significantly increased the mean decay time constant of baseline chloride recovery from 28.8±13.4 to 39.8±25.6 s (Figure 2e-f; n=6 slices at DIV9-12, 14 cells; paired t-test, t=-2.018, P=0.017). In contrast, bath application of WNK463 (1 µM for 15-20 min) significantly decreased the mean decay time constant from 52.5±26.2 to 32.8±24.9 s (Figure 2g-h; n=5 slices at DIV9-14, 8 of 10 cells; paired t-test, t=4.27, P=0.004). In two of ten cells, the exponential decay function did not fit the recovery of $[Cl^-]_i$ (not shown). In all cells that responded to GABA/L-Glu puff applications WNK463 also significantly reduced the amplitude of $[Cl^-]_i$ transients, which we tentatively attribute to enhanced Cl^- extrusion. Thus, the WNK-SPAK/ORS1 inhibitor WNK463 enhanced $[Cl^-]_i$ extrusion during recovery from GABA/L-Glu induced chloride transients.

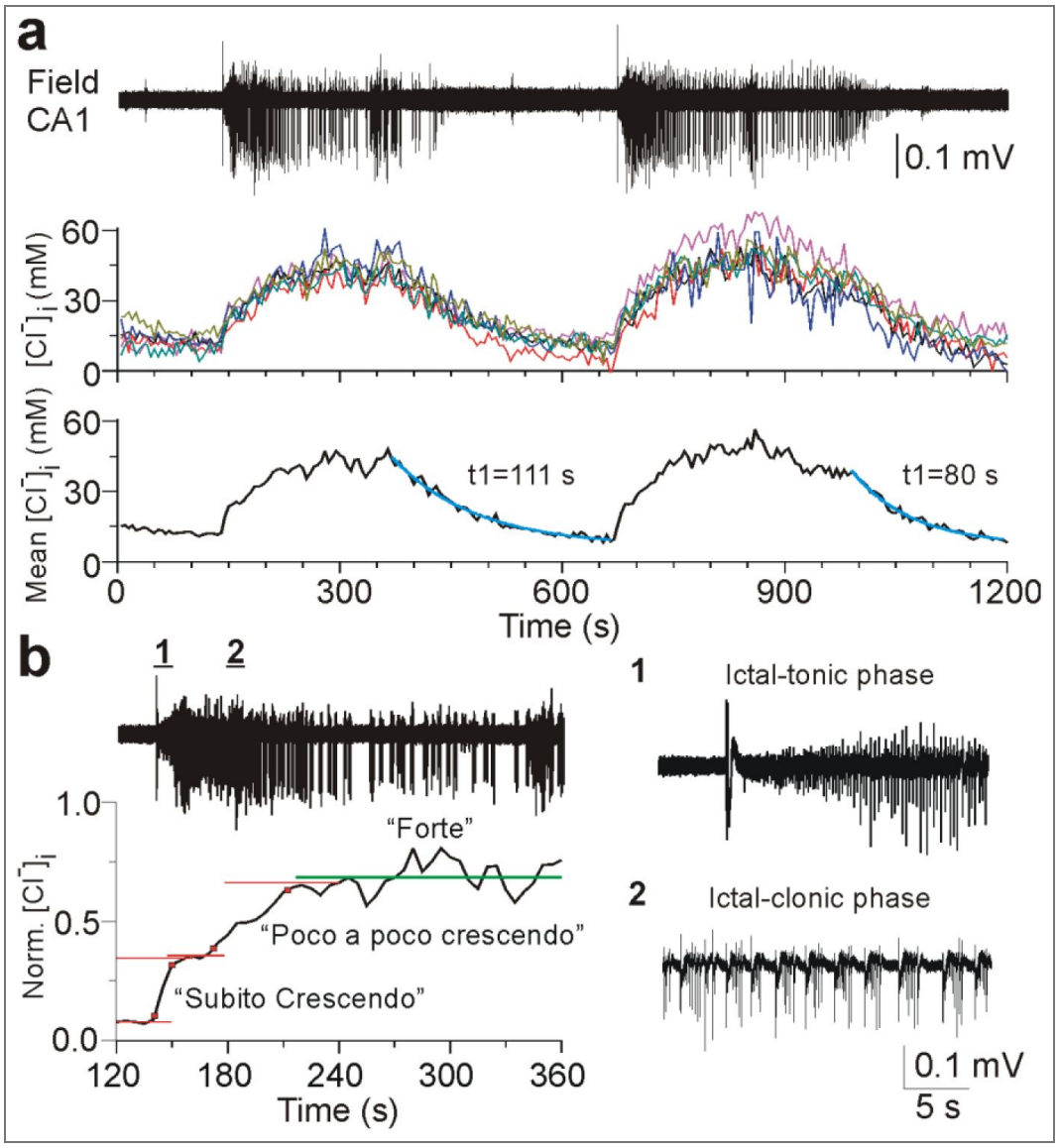

Figure 1. Neuronal chloride transients during spontaneous ictal-like discharges.

(**a**) Simultaneous extracellular field potential recording and two-photon fluorescence chloride imaging in the organotypic hippocampal slice at DIV18. Example of spontaneous recurrent ictal-like epileptiform discharges (ILDs) and corresponding $[Cl^-]_i$ transients in the CA1 pyramidal cells (n=6), and the mean $[Cl^-]_i$. $[Cl^-]_i$ progressively increased during "crescendo" phase of sustained ictal-tonic discharges, was relatively stable during "forte" phase of intermittent ictal-clonic discharges, and progressively decreased during "decrescendo" phase of secondary after-discharges and post-ictal depression (decay time constant (t1) 80-111 s). (**b**) Expansion of ILDs and mean $[Cl^-]_i$ changes normalized to values between 0 and 1 ([0, 1]). $[Cl^-]_i$ rapidly increased during hyper-synchronous onset of ILD ("subito crescendo") and subsequent sustained ictal-tonic discharges ("poco a poco crescendo") and was relatively stable during intermittent epileptiform discharges. (**b1-2**) Expansion of sustained ictal-tonic discharges and intermittent ictal-clonic epileptiform discharges.

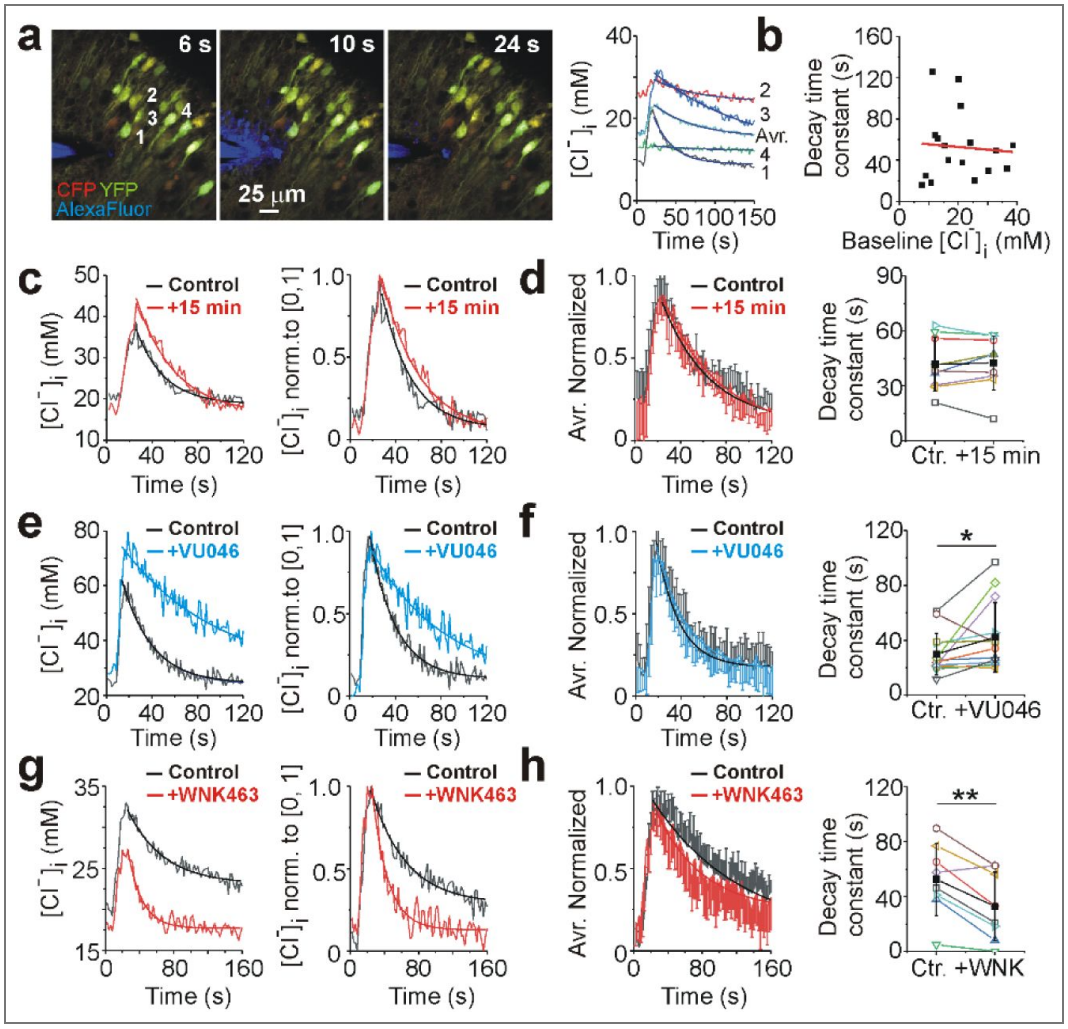

Figure 2. WNK-SPAK/OSR1 inhibitor WNK463 facilitated neuronal chloride extrusion.

(**a**) An illustration of the designed experiment to induce neuronal chloride transients in the CA1 pyramidal cells expressing sCLM. The puff micropipette filled with extracellular solution containing GABA (50 μM) and L-Glu (50 μM) was placed above the dendritic area of the neurons. Merged CFP (*red*) and YFP (*green*) fluorescent signals in subpopulation of neurons before (6 s), during (10 s) and after (24 s) GABA/L-Glu puff application. Alexa Fluo-594 (*blue*) was added for visualization. Corresponding $[Cl^-]_i$ transients induced by GABA/L-Glu puff application. Exponential decay fit ($y=y_0+A1\exp(-(x-x_0)/t1)$) was used to measure decay time constant (t1) of $[Cl^-]_i$ recovery in individual cells (1-4; *solid curves*). (**b**) Linier regression analysis revealed that decay time constant of $[Cl^-]_i$ recovery in individual cells was independent of the baseline $[Cl^-]_i$ and corresponding E_{GABA}. (**c-h**) $[Cl^-]_i$ transients, corresponding $[Cl^-]_i$ changes normalized to values between 0 and 1 and exponential decay curves in individual cells and averaged means (mean±SD) in control (**c, d**), before and during 1 μM VU0463271 application (**e, f**) and 1 μM WNK463 application (**g, h**). (**d**) In control, exponential decay time constant was not significantly different between two consecutive Cl^- transients. (**f**) The KCC2 antagonist VU0463271 significantly increased the mean decay time constant (*P<0.05, paired t-test). (**h**) The WNK-SPAC/OSR1 inhibitor WNK463 significantly decreased the mean decay time constant of chloride recovery (**P<0.01, paired t-test).

Next, we determined the net effects of WNK-SPAK/OSR1 catalytic activity inhibitor WNK463 on the frequency and duration of recurrent interictal- and ictal-like epileptiform discharges, baseline chloride changes, $[Cl^-]_i$ elevation and extrusion rates during ILDs, and the correlation between ionic and electrographic effects in *in vitro* model of post-traumatic epileptogenesis (Figures 3-5).

WNK463 abolished recurrent ILDs

Extracellular field potential recordings were performed in the CA1 pyramidal cell layer in the organotypic hippocampal slices at DIV12-19 before (control), during and after bath application of WNK463 (Figure 3a). Bath application of WNK463 (1 μM for 30 min) progressively reduced the mean frequency of ILDs from 7.33±3.7 to 0.17±0.41 ILD/10 min and abolished ILDs (Figure 3b; n=6 slices; One Way RM ANOVA: DF=53, F=15.18, P<0.001; Tukey test df=7.16, q=9.81, p<0.001). WNK463 substantially decreased the mean duration of ILDs from 0.32±0.16 to 0.04±0.05 min (DF=53, F=17.27, P<0.001; Tukey test: df=0.28, q=7.77, p<0.001). The corresponding mean power of electrical activity significantly decreased from 486.35±187.5 to 138.93±107.15 μV^2 (DF=53, F=21.74, P<0.001; Tukey test: df=347.4, q=10.7, p<0.001). However, WNK463 did not change the mean frequency and duration of periodic IEDs (Figure 3c; IED frequency: One Way RM ANOVA, DF=47, F=1.01, P=0.45; IED duration: DF=47, F=1.41, P=0.23). Thus, WNK463 progressively reduced the frequency, duration, and power of ILDs, and abolished recurrent ILDs.

WNK463 reduced activity-dependent interictal $[Cl^-]_i$ between ILDs

We next determined whether the anti-ictal effects of WNK463 (1 μM) correlate with changes in interictal $[Cl^-]_i$ and the rates of $[Cl^-]_i$ elevation and extrusion during recurrent ILDs (Figure 4). To clarify terminology, interictal (IED) $[Cl^-]_i$ is the cytoplasmic Cl^- concentration measured between ILDs. Baseline $[Cl^-]_i$ is the cytoplasmic Cl^- concentration measured in TTX. In line with previous studies (Lillis et al., 2012;Glykys et al., 2014;Dzhala and Staley, 2021), the median interictal $[Cl^-]_i$ transiently increased in all pyramidal cells from 25.75 (14.63-47.64) to 47.64 (25.79-88.32) mM during ILDs (Figure 4 a-c; n=4 slices at DIV12-19, 73 paired cells; Friedman RM ANOVA on Ranks, Chi-square=134.1, P<0.001; Tukey test: dr=105.6, q=9.56, p<0.05). Bath application of WNK463 abolished ILDs and corresponding $[Cl^-]_i$ transients and significantly reduced the median interictal $[Cl^-]_i$ to 23.37 (11.55-35.21) mM (dr=69.5, q=6.3, p<0.05). Interictal $[Cl^-]_i$ recovered to 26.06 (13.76-39.34) mM during washing out of WNK463 (dr=49.5, q=4.49, p<0.05). WNK463 induced changes in interictal $[Cl^-]_i$ were plotted as a function of initial interictal $[Cl^-]_i$ (Figure 4d). Linear regression analysis suggested a larger effect of WNK463 in neurons with higher initial interictal $[Cl^-]_i$ (A=11.2±1.4, B=-0.7±0.03; Pearson's r=-0.94, R^2=0.89). Thus, pharmacological inhibition of the WNK-SPAK/OSR1 catalytic activity by WNK463 leads to reduction in the interictal $[Cl^-]_i$ in neurons and negative shifts in the interictal E_{GABA}, increasing the net inhibition of neuronal network activity, and suppression of recurrent ILDs.

Pharmacological manipulations of the WNK-SPAK/OSR1-CCCs activity by WNK463 could produce anti-ictal effects that affect $[Cl^-]_i$ as a consequence of reduced ictal Cl^- loading, separately from the consequences of altered chloride transport (Dzhala and Staley, 2021). To estimate how direct anti-ictal effects might alter interictal $[Cl^-]_i$, we applied the sodium channel antagonist TTX (1 μM) to block synaptic activity and determined the effect of WNK463 on baseline $[Cl^-]_i$ in the presence of TTX (Figure 4e-g). TTX application rapidly blocks ILD activity directly, providing a means to assess the effects of the intensity of ILD activity on interictal $[Cl^-]_i$ levels separately from effects on Cl^- transport. TTX rapidly abolished ILDs and corresponding $[Cl^-]_i$ transients, and significantly reduced the median interictal $[Cl^-]_i$ from 22.5(16.06-26.94) to a baseline of 17.98 (11.94-21.36) mM (Figure 4e-f; N=4 slices at DIV14-16, 90 paired cells; Friedman RM ANOVA on Ranks, Chi-square=206.17, P<0.001; Tukey test: interictal $[Cl^-]_i$ compared to TTX, dr=111.5, q=9.1, p<0.05). Subsequent application of WNK463 (1 μM) in the continued presence of TTX did not significantly change the median baseline $[Cl^-]_i$ to 20.25(13.16-23.4) mM (dr=11.5, q=0.94, p>0.05) suggesting a contribution of activity-dependent $[Cl^-]_i$ accumulation during recurrent ILDs. However, the median baseline $[Cl^-]_i$ in the presence of WNK463+TTX remained significantly lower compared to

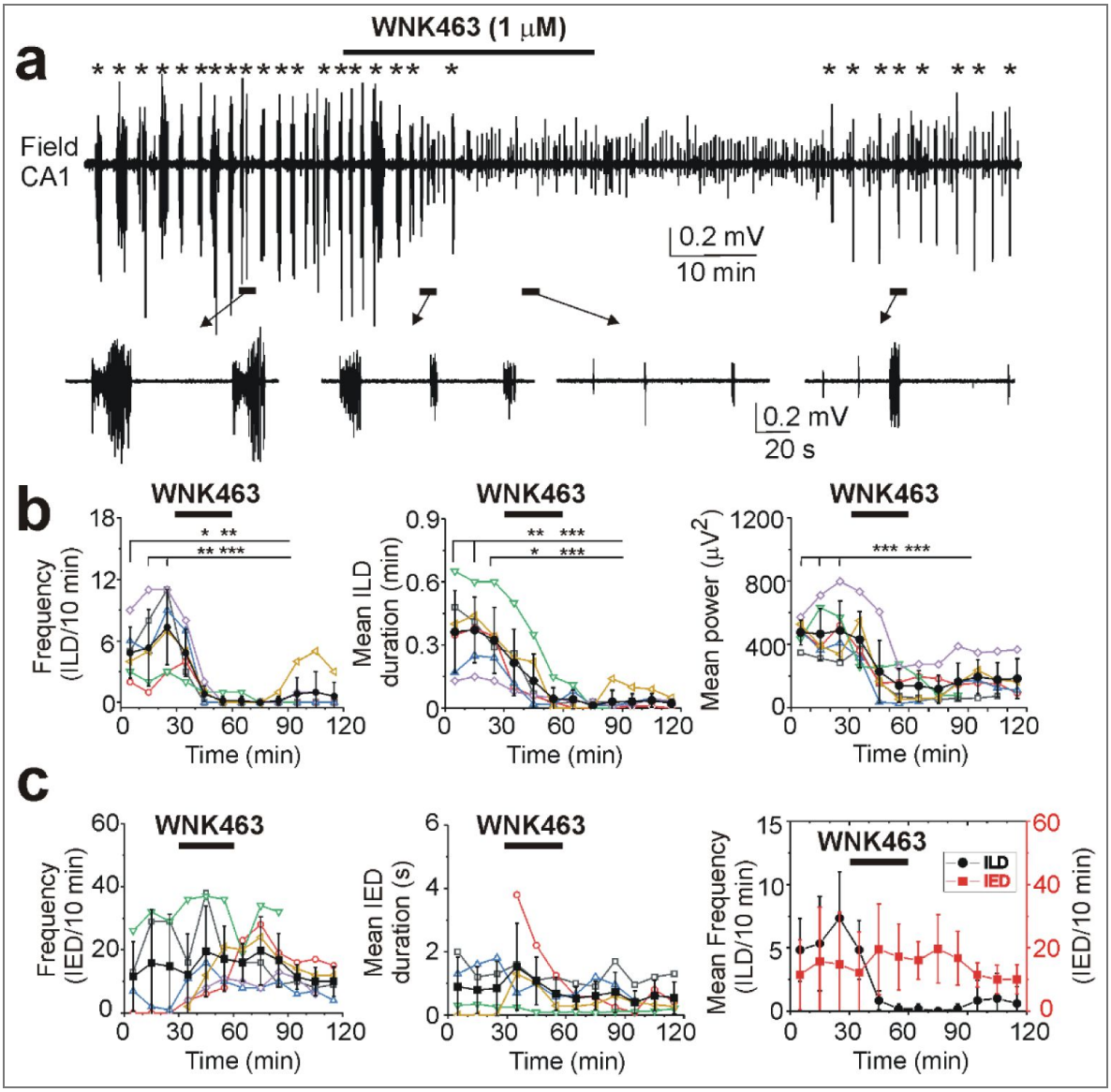

Figure 3. WNK-SPAK/OSR1 inhibitor WNK463 abolished recurrent ictal-like epileptiform discharges.

(**a**) Extracellular field potential recording in the CA1 pyramidal cell layer in the organotypic hippocampal slice at DIV21 before (control), during and after application of 1 μM WNK463 for 30 min. Expansion of recurrent ictal (ILDs) and interictal (IEDs) epileptiform discharges before, during and after application of WNK463. (**b, c**) Corresponding summary plots of the frequency and duration of recurrent ILDs (**b**) and IEDs (**c**) in individual slice cultures (DIV14-22, open symbols) and corresponding power of electrical activity in 10 min windows. Filled symbols indicate group mean ± SD. WNK463 (1 μM) progressively decreased the mean frequency, duration, and power of recurrent ILDs and abolished ILDs (*P<0.05; **P<0.01; ***P<0.001, One Way RM ANOVA, Tukey Test). (**c**) WNK463 (1 μM) did not significantly change the mean frequency and duration of periodic IEDs (P>0.05).

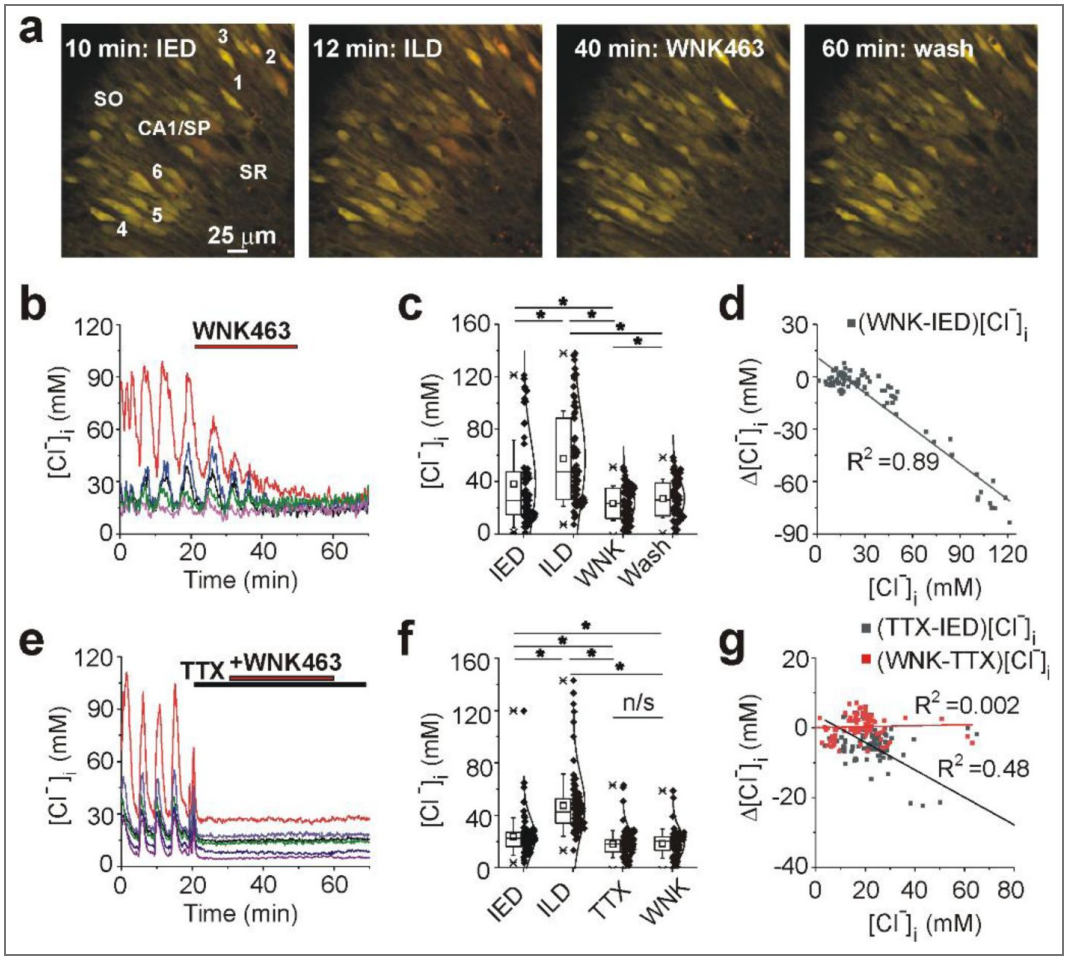

Figure 4. WNK463 progressively reduced activity-induced elevations in interictal $[Cl^-]_i$ and abolished neuronal Cl^- transients.

(**a**) Two-photon microscopy images of Clomeleon in the CA1 pyramidal cell layer in the organotypic hippocampal slice *in vitro* (DIV19). Merged CFP (*red*) and YFP (*green*) fluorescent signals before, during and after WN463 (1 µM for 30 min) application. (**b**) Corresponding $[Cl^-]_i$ changes in individual cells are plotted as a function of time. WNK463 abolished recurrent ILDs and corresponding Cl^- transients. (**c**) Baseline $[Cl^-]_i$ distribution in subpopulations of neurons before (IED and ILD phases), during and after application of WNK463. Box (*left*) + data (*right*) plots correspond to median (25%–75%) $[Cl^-]_i$ in individual cells (filled symbols) and their Gaussian distribution curves; open squares and whisker range indicate mean±SD. WNK463 significantly reduced the median interictal $[Cl^-]_i$ (*P<0.05; Friedman RM ANOVA on Ranks). (**d**) Corresponding interictal $[Cl^-]_i$ changes induced by WNK463. Data were fitted with a linier regression fit. (**e**) WNK463 (1 µM) did not change baseline $[Cl^-]_i$ when synaptic activity had already been suppressed with the sodium channel blocker TTX (1 µM). (**f**) Baseline $[Cl^-]_i$ distribution and corresponding $[Cl^-]_i$ changes induced by TTX and WNK463 in the presence of TTX (*P<0.05; Friedman RM ANOVA on Ranks). (**g**) Corresponding interictal $[Cl^-]_i$ changes in individual cells induced by TTX (black symbols and line) and baseline $[Cl^-]_i$ changes induced by WNK463 in the presence of TTX (red symbols and line). Data were fitted with a linear regression fit.

the no-TTX control interictal condition (dr=100, q=8.16, p<0.05). TTX induced changes in interictal $[Cl^-]_i$ were plotted as a function of initial interictal $[Cl^-]_i$, and WNK463 induced changes in baseline $[Cl^-]_i$ were plotted as a function of preceding baseline $[Cl^-]_i$ in the presence of TTX (Figure 4g). Linear regression analysis revealed that the rate of interictal $[Cl^-]_i$ reduction induced by TTX was greater than the effect of WNK463 on baseline $[Cl^-]_i$ in the presence of TTX (Figure 4g: $\Delta[Cl^-]_i$ (TTX) vs interictal $[Cl^-]_i$ in control: A=3.68±1.2, B=-0.39±0.04, Pearson's r=-0.69, R^2=0.48; $\Delta[Cl^-]_i$ (WNK463+TTX) vs baseline $[Cl^-]_i$ in the presence of TTX: A=0.026±0.7, B=0.014±0.03, Pearson's r=0.043, R^2=0.002). Thus, pharmacological inhibition of the WNK-SPAK/OSR1 catalytic activity by WNK463 leads to both increased CCC-mediated Cl^- export as well as indirect decreases in Cl^- influx during ictal network activity that are replicated by TTX. Both effects increase the net inhibition of neuronal network activity and suppression of recurrent ILDs.

WNK463 progressively enhanced neuronal chloride extrusion during ILDs

As another assessment of the effects of WNK-SPAK/OSR1 inhibition on neuronal chloride transport activity during suppression of recurrent ILDs, we compared the rise-time of $[Cl^-]_i$ elevation and decay time constant of $[Cl^-]_i$ extrusion during recurrent ILDs in control, and before and during application of WNK463 (1 µM) (Figure 5a, c). In control conditions, the mean rise time of $[Cl^-]_i$ elevation and the mean decay time constant of $[Cl^-]_i$ extrusion during recurrent ILDs were relatively stable in line with the frequency and duration of recurrent ILDs (n=5 slices at DIV13-18, n=32 paired cells; Rise time: One Way RM ANOVA, DF=31, F=1.592, P=0.212; Decay time constant: DF=31, F=3.35, P=0.448). WNK463 application progressively depressed recurrent ILDs (Figure 3), providing a means to assess the effects of WNK463 on neuronal $[Cl^-]_i$ transients and kinetics. Bath application of WNK463 (1 µM) insignificantly reduced the mean rise time of chloride accumulation during onset of ILDs from 27.26±15.8 s in control, before WNK463 application, to 20.54±10.1 s over 10 to 20 min WNK463 application (Figure 5e; n=5 slices at DIV12-19, 25 paired cells; One Way RM ANOVA, DF=24, F=2.77, P=0.032; Tukey test: df=6.72, q=2.43, p>0.05). Recurrent ILDs and $[Cl^-]_i$ transients were suppressed over 20 to 30 min WNK463 application (Figures 3, 5). The corresponding exponential decay time constant (t1) of $[Cl^-]_i$ extrusion (recovery) during ILDs significantly decreased from the mean 85.65±53.27 s in control to 31.98±21.4 s in the presence of WNK463 (Figure 5e; One Way RM ANOVA: DF=24, F=12.43, P<0.001; Tukey Test: df=53.67, q=8.41, p<0.001). In contrast, application of KCC2 inhibitor VU0463271 (1 µM) increased the decay time constant of $[Cl^-]_i$ extrusion during recurrent ILDs and corresponding chloride transients in line with increased duration of recurrent ILDs and transition to electrical *status epilepticus* (Dzhala and Staley, 2021). Thus, the WNK-SPAK/OSR1 pathway can regulate the maximum velocity of CCCs during intense activation of the $GABA_A$-R and $[Cl^-]_i$ accumulation as occurs during prolonged ILDs. Progressively decreased duration and power of recurrent ILDs in the presence of the WNK-SPAK/OSR1 blocker WNK463 would be expected to decrease Cl^- influx, and correlates with decreased rise time, amplitude, and duration of $[Cl^-]_i$ elevation, consistent with both a decrease in Cl^- influx and an enhanced extrusion rate of $[Cl^-]_i$ (Figure 5f).

WNK463 had no effects in the presence of the $GABA_A$-receptor antagonist and CCCs inhibitors

We next used pharmacological tools to determine whether $GABA_A$-R block prevents the anti-ictal effects of the WNK-SPAK/OSR1 blocker WNK463 (Figure 6a-c). In line with previous studies (Dzhala and Staley, 2021), bath application of the $GABA_A$-R antagonist SR95531 (10 µM) rapidly abolished ILDs and corresponding $[Cl^-]_i$ transients (Lillis et al., 2012), and induced large amplitude and 1-2 s duration interictal-like epileptiform discharges (IEDs) (Figure 6a, b; n=6 slices at DIV13 to DIV17, ILD frequency: Friedman RM ANOVA on Ranks: Chi-square=57.18 with 11 degrees of freedom, P=<0.001; Dunn's Test: dr=6.33, q=3.04, p<0.05). Subsequent application of WNK463 (1 µM), in the continued presence of SR95531, did not significantly change the mean frequency and duration of epileptiform discharges, and the corresponding mean power of electrical activity in 10 min windows (Figure 6a-c; IED frequency: Friedman RM ANOVA on

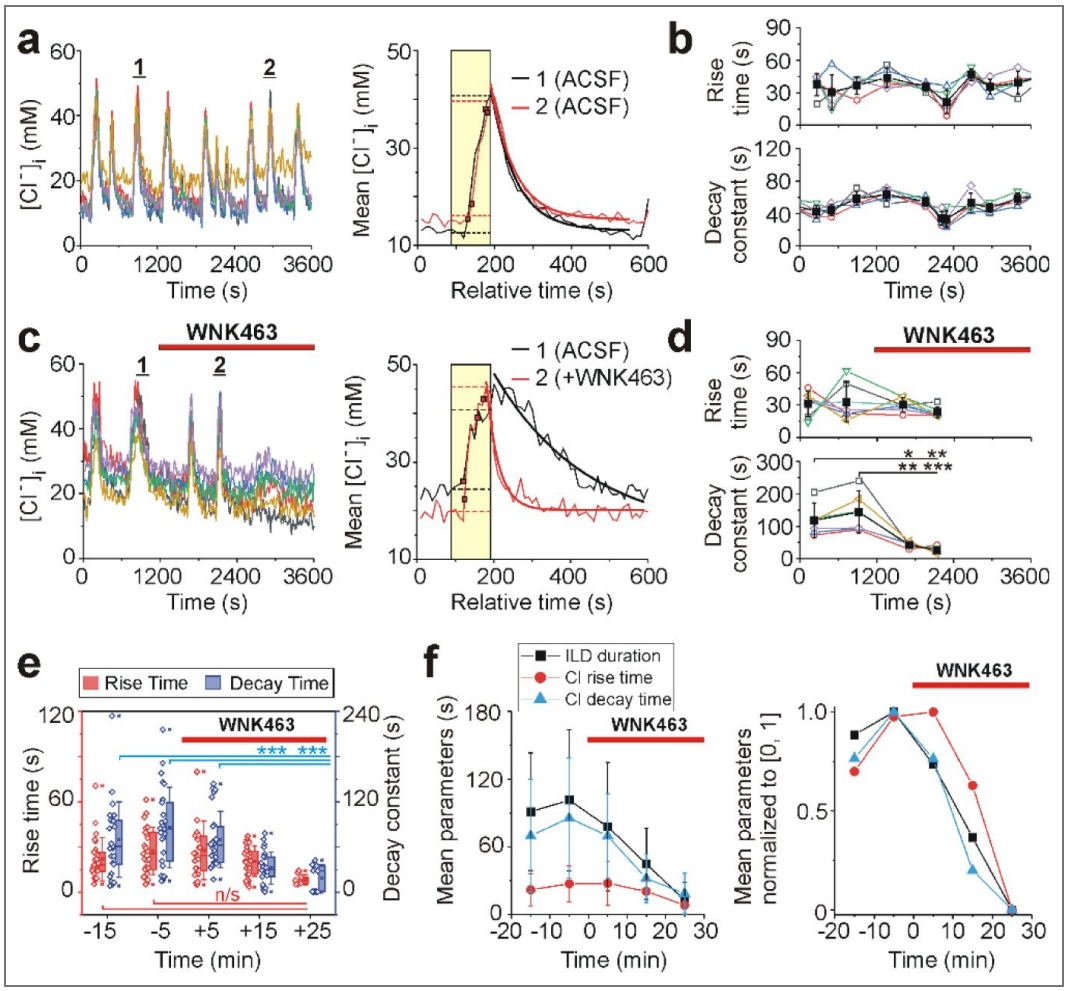

Figure 5. Effects of the WNK-SPAK/OSR1 blocker WNK463 on neuronal chloride transients during recurrent ictal-like epileptiform discharges.

(**a, c**) Neuronal Cl^- changes in individual cells as a function of time and corresponding mean $[Cl^-]_i$ transients in control ACSF (**a1-2**), and before and during WNK463 (1 μM) application (**c1-2**). (**b, d**) Corresponding rise time and decay time constant of $[Cl^-]_i$ transients in individual cells (open symbols) as a function of time in control (**b**), and before and during WNK463 application (**d**). Filled symbols indicate group mean ± SD. WNK463 progressively decreased the mean decay time constant of $[Cl^-]_i$ transients (*P<0.05, **P<0.01, ***P<0.001; One Way RM ANOVA). (**e**)$[Cl^-]_i$ rise time and decay time constant of neuronal chloride transients in individual cells before and during WNK463 application (n/s corresponds to P>0.05, ***P<0.001, One Way RM ANOVA, Tukey's test). Box (*right*) + data (*left*) plots correspond to median (25%–75%) $[Cl^-]_i$ in individual cells (open symbols); open squares and whisker range indicate mean±SD. (**f**) The mean ILD duration, corresponding $[Cl^-]_i$ rise time and decay time constant of neuronal chloride transients, and corresponding normalized parameters before and during WNK463 application. WNK463 progressively reduced the mean duration of ILDs (black symbols) in line with enhanced Cl^-extrusion rate (blue symbols).

Ranks, Chi-square=16.1 with 11 degrees of freedom, P=0.147; Power: One Way RM ANOVA, DF=65, F=1.08, P=0.4). These data suggest that the anti-ictal effects of the WNK-SPAK/OSR1 blocker WNK463 require activation of $GABA_A$-Rs. However, we cannot rule out that cation-chloride cotransporter (CCC)-mediated Cl^- export and $GABA_A$-R activity is not as critical to the termination of short-duration IEDs (Staley et al., 1998) as to the termination of longer-lasting ILDs.

High concentrations of CCC inhibitors have large anticonvulsant effects (Hochman et al., 1995;Dzhala and Staley, 2021). We also evaluated whether CCCs were necessary for the anti-ictal effects of WNK463 (Figure 6d-f). Under similar experimental conditions (DIV12 to DIV16), bath application of a high concentration of bumetanide (0.5 mM) that nonspecifically blocks CCCs (NKCC1 and KCC2-3) (Payne, 1997) significantly reduced the mean frequency of spontaneous ILDs from 3±0.89 to 0.83±0.75 ILD/10 min. Subsequent application of WNK463 (1 μM) in the continued presence of 0.5 mM bumetanide did not significantly change the mean frequency of ILDs to 0.5±0.84 ILD/10 min (Figure 6e; N=6 slices; One Way RM ANOVA: DF=71, F=9.71, P<0.001; Tukey Test: control compared to bumetanide, df=2.17, q=7.2, P<0.001; control compared to WNK463 in the presence of bumetanide, df=2.5, q=8.3, P<0.001; bumetanide compared to WNK463 in the presence of bumetanide, df=0.33, q=1.1, P=1.00). The corresponding mean power of electrical activity significantly decreased from 644±153.97 μV^2 in control to 238.49±127.18 μV^2 during bumetanide application, and consecutive application of WNK463 in the presence of bumetanide did not significantly change the mean power of electrical activity to 215.3±128.9 μV^2 (Figure 6e; One Way RM ANOVA: DF=59, F=15.16, P<0.001; Tukey Test: control compared to bumetanide, df=405.53, q=7.4, P<0.001; control compared to WNK463 in the presence of bumetanide, df=428.69, q=7.8, P<0.001; bumetanide compared to WNK463 in the presence of bumetanide, df=23.16, q=0.42, P=0.987).

The mean effect of WNK463 on the power of epileptiform activity (percent of treatment-preceding power) was significantly different as the corresponding effects of WNK463 in the presence of 10 μM SR95531 or 0.5 mM bumetanide (Figure 6f; One Way ANOVA, DF=19, F=62.2, P<0.001; Holm-Sidak Test: WNK463+SR95531 compared to WNK463, df=80.47, t=10.83, P<0.001; WNK463+Bum compared to WNK463, df=58.27, t=7.53, P<0.001). These results suggest that the anti-ictal action of WNK463 requires functional $GABA_A$-Rs and is dependent on CCCs activity, and greatly exceeds the anti-ictal effects of specific blockers of NKCC1 transport activity or activators of KCC2 transport activity under similar experimental conditions (Dzhala and Staley, 2015;Dzhala and Staley, 2021). However, the WNK effect is in line with the anticonvulsant effects of very high, non-specific concentrations of CCC antagonists (Hochman et al., 1995;Dzhala and Staley, 2021).

NKCC1 inhibition did not prevent the anti-ictal effects of WNK463

The WNK-SPAK/OSR1 catalytic pathway inhibitor WNK463 reduces phosphorylation of the WNK1 downstream targets SPAK/OSR1 (Yamada et al., 2017) and thereby inhibits NKCC1 and KCC2 phosphorylation (de Los et al., 2014), resulting in inhibition of NKCC1 and stimulation of KCC2 activity. The relative contribution of NKCC1 and KCC2 transport activity to the anti-ictal effects of WNK463 is not known. We used pharmacological tools to determine whether NKCC1 inhibition by bumetanide (10 μM) and KCC2 inhibition by VU0463271 (1 μM) prevents the anti-ictal effects of WNK463 (Figure 7).

Bath application of bumetanide (10 μM) did not significantly change the mean frequency of recurrent ILDs from 4.5±1.2 to 3.2±2.04 ILD/10 min, and subsequent application of WNK463 (1 μM) in the continued presence of bumetanide (10 μM) reduced the mean frequency of ILDs to 0.67±1.2 ILD/10 min (Figure 7b; n=6 slices at DIV16 to 21; One Way RM ANOVA: DF=59, F=6.11, P<0.001; Tukey Test: control compared to bumetanide, df=1.33, q=2.51, p=0.75; control compared to WNK463+bumetanide, df=3.83, q=7.16, p<0.001; bumetanide compared to WNK463+bumetanide, df=2.5, q=4.7, p=0.05). Bumetanide (10 μM) did not significantly change the mean power of corresponding electrical activity from 624.8±164.5 to 467.71±149.83 μV^2, and consecutive application of WNK463 in the presence of bumetanide significantly decreased the mean power of electrical activity to 194.84±138.94 μV^2 (Figure 7b; One Way RM ANOVA: DF=62, F=8.04, P<0.001; Tukey Test: control compared to bumetanide, df=157.11, q=2.72, p=0.59; control compared to

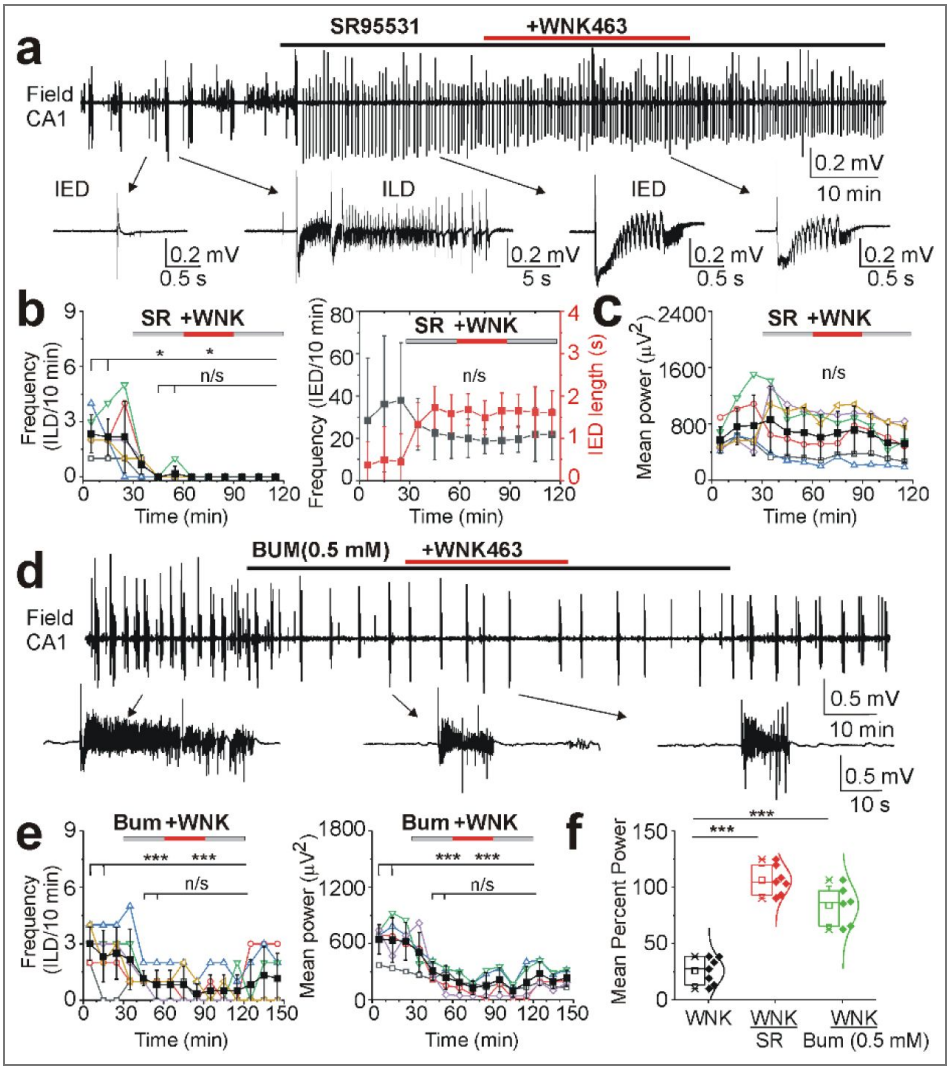

Figure 6. WNK463 had no effects in the presence of the $GABA_A$-receptor antagonist and CCCs inhibitors

(**a, d**) Extracellular field potential recordings in the CA1 pyramidal cell layer in the organotypic hippocampal slices *in vitro*. Expansion of recurrent interictal (IEDs) and ictal (ILDs) epileptiform discharges in control and during drug applications. (**b, c**) Application of the $GABA_A$-R antagonist SR95531 (10 μM) abolished spontaneous ILDs and induced large amplitude IEDs. Subsequent application of WNK463 (1 μM) in the presence of SR95531 did not change the mean frequency and duration of epileptiform discharges and corresponding power of electrical activity (n/s – P>0.05; *P<0.05; Friedman RM ANOVA on Ranks, Dunn's test). (**e**) Cation-chloride cotransporter blocker bumetanide (0.5 mM) reduced the mean frequency of ILDs, corresponding power of electrical activity, and prevented the anti-ictal effects of WNK463 (n/s – P>0.05; *P<0.05; ***P<0.001; One Way RM ANOVA, Tukey test). (**f**) The mean effect of WNK463 on the power of epileptiform activity (percent of treatment-preceding power) was significantly different as the corresponding effects of WNK463 in the presence of 10 μM SR95531 or 0.5 mM bumetanide (***P<0.001; One Way ANOVA, Holm-Sidak Test).

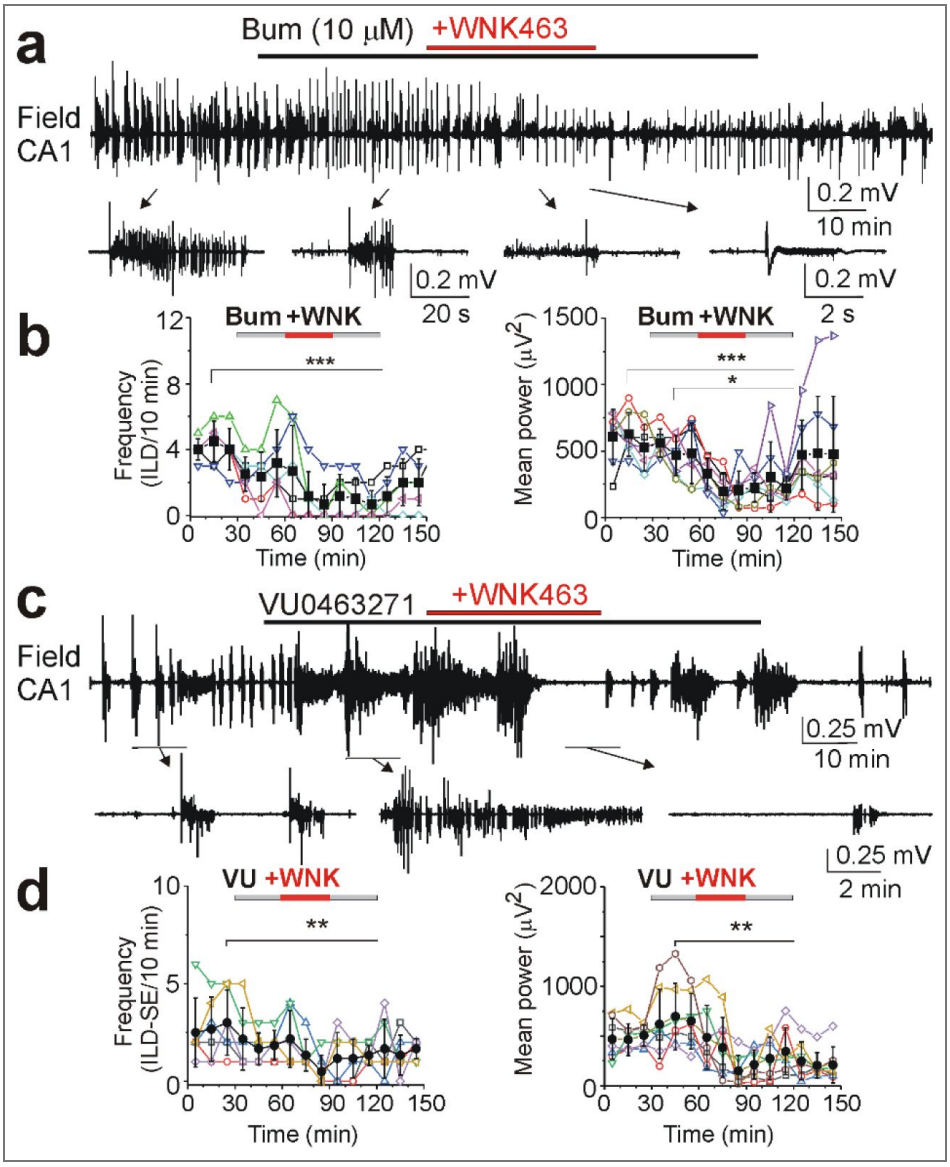

Figure 7. Anti-ictal effects of WNK463 in the presence of NKCC1 blocker bumetanide and KCC2 blocker VU0463271.

(**a, c**) Extracellular field potential recordings in the CA1 pyramidal cell layer in the organotypic hippocampal slices *in vitro*. WNK463 (1 μM) was applied in the presence of (**a**) NKCC1 blocker bumetanide (10 μM) and (**c**) KCC2 blocker VU0463271 (1 μM). Expansion of epileptiform discharges before and during drugs applications. (**b**) WNK463 application in the presence of bumetanide significantly reduced the mean frequency of recurrent ILDs in control and the mean power of electrical activity. (**d**) WNK463 in the presence of VU0463271 significantly reduced the mean frequency of ILDs in control and the mean power of electrical activity in the presence of VU0463271 alone (*p<0.05, **p<0.01, ***p<0.001; One-Way RM ANOVA, Tukey test).

WNK463+bumetanide, df=429.9, q=7.46, p<0.001; bumetanide compared to WNK463+bumetanide, df=272.87, q=4.73, p=0.039). On average, WNK463 application in the presence of bumetanide significantly reduced the mean power of electrical activity in the presence of bumetanide (10 μM) alone by 59.9±21.1%. These data indicate that the effect of WNK463 is not mediated solely by effects on NKCC1 activity.

KCC2 inhibition did not prevent the anti-ictal effects of WNK463

We next determined whether KCC2 inhibition affects the anti-ictal effects of WNK463 (Figure 7c). Under similar experimental conditions (DIV16 to DIV21), bath application of KCC2 inhibitor VU0463271 (1 μM) reduced the mean frequency of ILDs from 3±1.67 to 1.83±0.75 ILD/10 min, and subsequent application of WNK463 (1 μM), in the continued presence of VU0463271, reduced the mean frequency of ILDs to 0.5±0.84 ILD/10 min (Figure 7d; n=6 slices, One Way RM ANOVA: DF=59, F=3.46, P=0.003; Tukey Test: control compared to VU0463271, df=1.17, q=2.86, p=0.59; control compared to WNK463+VU0463271, df=2.5, q=6.13, p=0.003; VU0463271 compared to WNK463+ VU0463271, df=1.33, q=3.27, p=0.4). VU0463271 increased the mean power of corresponding electrical activity from 498.37±148.11 μV^2 in control to 697.55±335.23 μV^2, and consecutive application of WNK463, in the presence of VU0463271, significantly decreased the mean power of electrical activity to 151.67±157.47 μV^2 (Figure 7d; One Way RM ANOVA: DF=71, F=4.26, P<0.001; Tukey Test: VU0463271 compared to control, df=199.18, q=2.38, p=0.86; control compared to WNK463+VU0463271, df=346.7, q=4.15, p=0.15; VU0463271 compared to WNK463+VU0463271, df=545.9, q=6.53, p=0.001). On average, WNK463 application in the presence of VU0463271 reduced the mean power of electrical activity in the presence of VU0463271 alone by 44.8±32.3%. These results indicate that the anti-ictal effects of WNK463 are not mediated solely by effects on KCC2 activity and are likely due to coherent inhibition of NKCC1 and activation of KCC2.

siRNA targeted Slc12a2 or Slc12a5 gene silencing did not prevent the anti-ictal effects of WNK463

We next determined whether small-interfering RNA (siRNA) targeted gene silencing of either Slc12a2 (NKCC1) or Slc12a5 (KCC2) individually prevent or reduce the anti-ictal effects of WNK463, in line with pharmacological inhibition of NKCC1 and KCC2. To assess uptake of siRNA, age-matched organotypic hippocampal slices were prepared, cultured and incubated in corresponding siRNA delivery medium.. After 72 hours of incubation with green (fluorescein) non-targeting siRNA (DIV9-11), uptake of siRNA was visible during an additional 24+ hours incubation in standard culture medium (Figure 8a). The most prominent and intense fluorescence was observed in cells of *stratum radiatum* and *stratum pyramidale* layer, indicating an uptake of siRNA. n. Extracellular field potential recording in the CA1 and CA3 pyramidal cell layer in the siRNA-treated organotypic hippocampal slices revealed spontaneous multiple unit activity and population neuronal network activity, including short interictal-like discharges and prolonged ictal-like discharges (Figure 8b).

Previously published data revealed that siRNA targeted Slc12a2 gene silencing reduced NKCC1 expression and limited injury-induced changes in neuronal volume and chloride (Bahari et al., 2024). In all three age-matched groups of organotypic hippocampal slices cultured and treated for 72 hours (DIV9-11) with non-targeting siRNA (control), Slc12a2 siRNA (NKCC1) and Slc12a5 siRNA (KCC2), immunohistochemistry using specific antibodies revealed NKCC1 and KCC2 expression, in line with previous reports (46, 117). In groups of slices treated with targeting Slc12a2 siRNA or Slc12a5 siRNA, we found a significant reduction of primary NKCC1 (n=9 slices; Mann-Whitney Rank Sum Test, U Statistic=10, P=0.014) or KCC2 (n=9 slices; Mann-Whitney Rank Sum Test, U Statistic=1.000, P<=0.001) antibody staining and protein expression relative to 4',6-diamidino-2-phenylindole (DAPI) staining (Figure 8 c, d).

In all corresponding age-matched (DIV12-14) groups of organotypic hippocampal slices treated with siRNAs, electrical extracellular filed potential recording revealed spontaneous interictal- and ictal-like epileptiform discharges (Figure 8 e-j). In a control group of slices treated with non-targeting siRNA, bath application of WNK463 (1 μM for 30 min) progressively reduced the mean

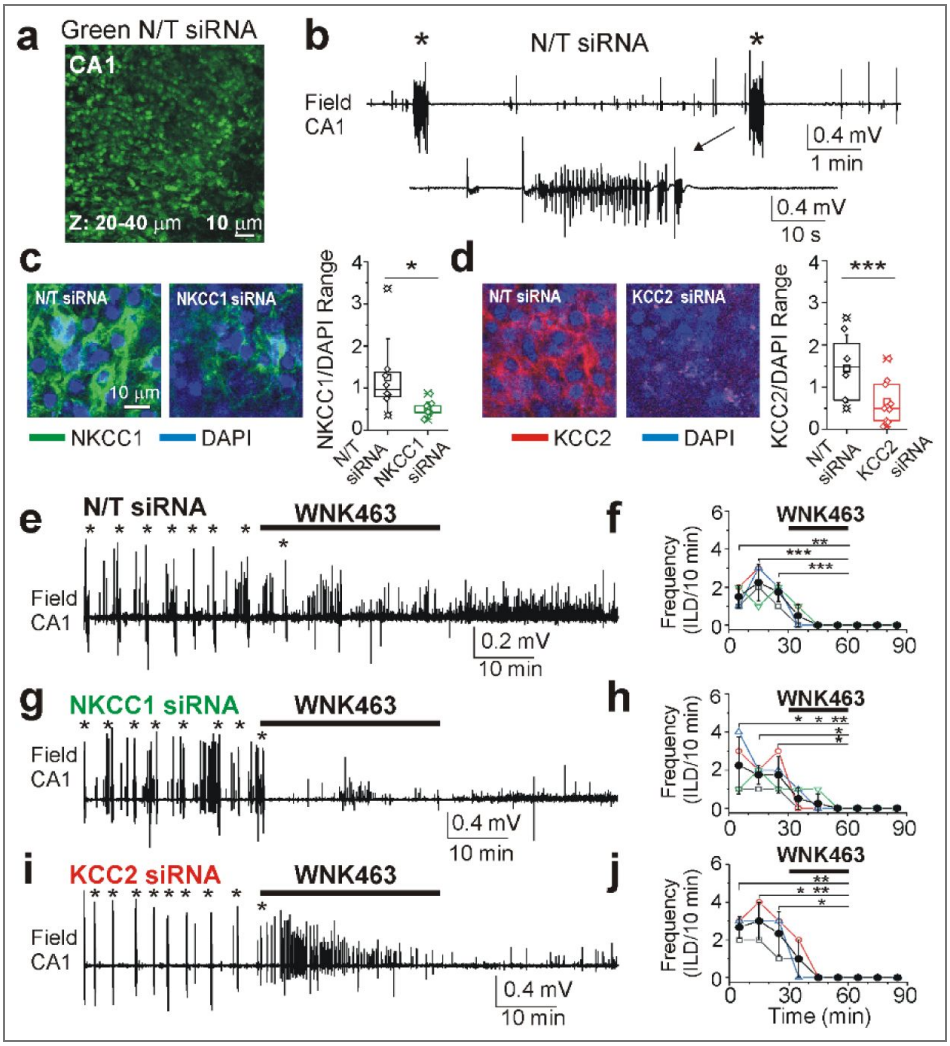

Figure 8. siRNA targeted Slc12A2 (NKCC1) and Slc12a5 (KCC2) gene silencing did not prevent the anti-ictal effects of WNK463.

(**a**) Cellular penetration by Accell green (fluorescein) non-targeting siRNA in the organotypic hippocampal slice *in vitro* at DIV12. (**b**) Simultaneous extracellular field potential recordings in the CA1 pyramidal cell layer revealed spontaneous multiple unit activity (MUA), interictal epileptiform discharges (IEDs) and ictal-like epileptiform discharges (ILDs). Expansion of recurrent ILD during recordings. (**c, d**) NKCC1 (green) and KCC2 (red) antibodies overlaid with 4',6-diamidino-2-phenylindole (DAPI) staining (blue) in control (N/T siRNA) and NKCC1 and KCC2 siRNA treated organotypic hippocampal slices. Optical density of NKCC1 and KCC2 immunostaining relative to DAPI staining revealed significant siRNA targeted Slc12A2 and Slc12a5 gene silencing and protein expression (*P<0.05;***P<0.001; Mann-Whitney test on ranks). (**e, f**) WNK463 (1 μM) abolished spontaneous ILDs (marked by asterisks) in control slices treated with non-targeting (N/T) siRNA. (**g, h**) WNK463 (1 μM) abolished spontaneous ILDs (marked by asterisks) in slices treated with Slc12a2 (NKCC1) siRNA. (**i, j**) WNK463 (1 μM) abolished spontaneous ILDs (marked by asterisks) in slices treated with Slc12a5 (KCC2) siRNA (*P<0.05, **P<0.01, ***P<0.01, One-Way RM ANOVA, Tukey test).

frequency of recurrent ILDs from 2.25±0.96 ILD/10 min in control ACSF (10 to 20 min) to 0.5±0.58 ILD/10 min (0 to 10 min over WNK463 application), and abolished recurrent ILDs (Figure 8e, f; n=4 slices; One Way RM ANOVA: DF=23, F=13.32, P<0.001; Tukey Test: Control vs WNK463 (0 to10 min over application), df=1.75, q=6.64, P=0.003; Control vs WNK463 (20 to 30 min over application), df=2.25, q=8.54, P<0.001). In slices treated with Slc12a2 siRNA (NKCC1), bath application of WNK463 (1 μM for 30 min) progressively reduced the mean frequency of recurrent ILDs from 1.75±0.5 ILD/10 min in control ACSF (10 to 20 min) to 0.25±0.5 ILD/10 min (10 to 20 min over WNK463 application), and abolished recurrent ILDs (Figure 8g, h; n=4 slices; One Way RM ANOVA: DF=23, F=6.29, P=0.002; Tukey Test: Control vs WNK463 (20 to 30 min over application), df=1.75, q=4.65, P=0.04). In slices treated with Slc12a5 siRNA (KCC2), bath application of WNK463 (1 μM for 30 min) progressively reduced the mean frequency of recurrent ILDs from 3±1 ILD/10 min in control ACSF (10 to 20 min) to 1±1 ILD/10 min during WNK463 application, and abolished recurrent ILDs (Figure 8i, j; n=3 slices; One Way RM ANOVA: DF=14, F=10.21, P=0.003; Tukey Test: Control vs WNK463 (0 to 10 min over application), df=2, q=5.1, P=0.04; Control vs WNK463 (20 to 30 min over application), df=3, q=7.61, P=0.004). Thus, siRNA targeted gene silencing of either Slc12a2 or Slc12a5 individually did not prevent or reduce the anti-ictal effects of WNK463, in line with pharmacological inhibition of NKCC1 and KCC2 (Figure 7).

Simultaneous NKCC1 and KCC2 inhibition reduced the anti-ictal effects of WNK463

We next determined whether simultaneous inhibition of NKCC1 and KCC2 cotransport prevents the anti-ictal effects of WNK463 (Figure 9). Bath application of NKCC1 inhibitor bumetanide (10 μM) in combination with KCC2 inhibitor VU0463271 (1 μM) significantly reduced the mean frequency of ILDs, and consecutive application of WNK463 (1 μM) in the presence of combination of bumetanide and VU0463271 (Bum+VU) insignificantly reduced the mean frequency of ILDs (Figure 9b; n=5, One Way RM ANOVA: DF=74, F=6.1, P<0.001; Tukey Test: control compared to Bum+VU: df=2.8, q=5.07, P=0.04; control compared to WNK463 in the presence of Bum+VU: df=3.2, q=5.8, p=0.01; Bum+VU compared to WNK463 in the presence of Bum+VU: df=0.4, q=0.72, p=1.0). The corresponding power of electrical activity was reduced from a mean 955.25±335.72 μV^2 in control to 885.16±169.25 μV^2 during simultaneous bumetanide and VU0463271 application, and to 349.13±174.14 μV^2 during consecutive application of WNK463 in the presence of bumetanide and VU0463271(Figure 9b; N=7, One Way RM ANOVA: DF=84, F=3.72, P<0.001; Tukey Test: control compared to Bum+VU, df=70.1, q=0.65, P=1.0; control compared to WNK463 in the presence of Bum+VU, df=606.12, q=5.6, P=0.012; Bum+VU compared to WNK463 in the presence of Bum+VU, df=536.03, q=4.95, P=0.04). Thus, simultaneous inhibition of NKCC1 and KCC2 did not prevent the anti-ictal effect of WNK463.

We compared the mean effects of WNK463 on the power of electrical activity in control conditions with the corresponding effects of WNK463 in the presence of NKCC1 and KCC2 inhibitors (Figure 9c). On average, WNK463 significantly reduced the mean power of electrical activity to 25.77±11.8 percent of control, and the mean anti-ictal effects of WNK463 were not significantly different from the corresponding effects of WNK463 in the presence of NKCC1 inhibitor bumetanide (10 μM), or in the presence of KCC2 inhibitor VU0463271 (1 μM) (Figure 9c; One Way ANOVA, DF=32, F=6.5, P<0.001; Holm-Sidak method, WNK463+Bum compared to WNK463: df=14.3, t=1.22, P=0.24; WNK463+VU compared to WNK463: df=29.01, t=2.34, p=0.029). However, simultaneous inhibition of NKCC1 and KCC2 by the combination of bumetanide (10 μM) and VU0463271 (1 μM) significantly reduced the anti-ictal effects of WNK463 (Figure 9c; WNK463 in the presence of 10 μM Bumetanide+VU0463271 compared to WNK463: df=43.5, t=3.5, p=0.002). These results suggest that the anti-ictal effects of WNK-SPAK/OSR1 inhibitor WNK463 are mainly due to downstream interactions with NKCC1 inhibition and KCC2 activation, and with additional effects due to interactions with an unidentified Cl^-transporter, exchanger, or channel.

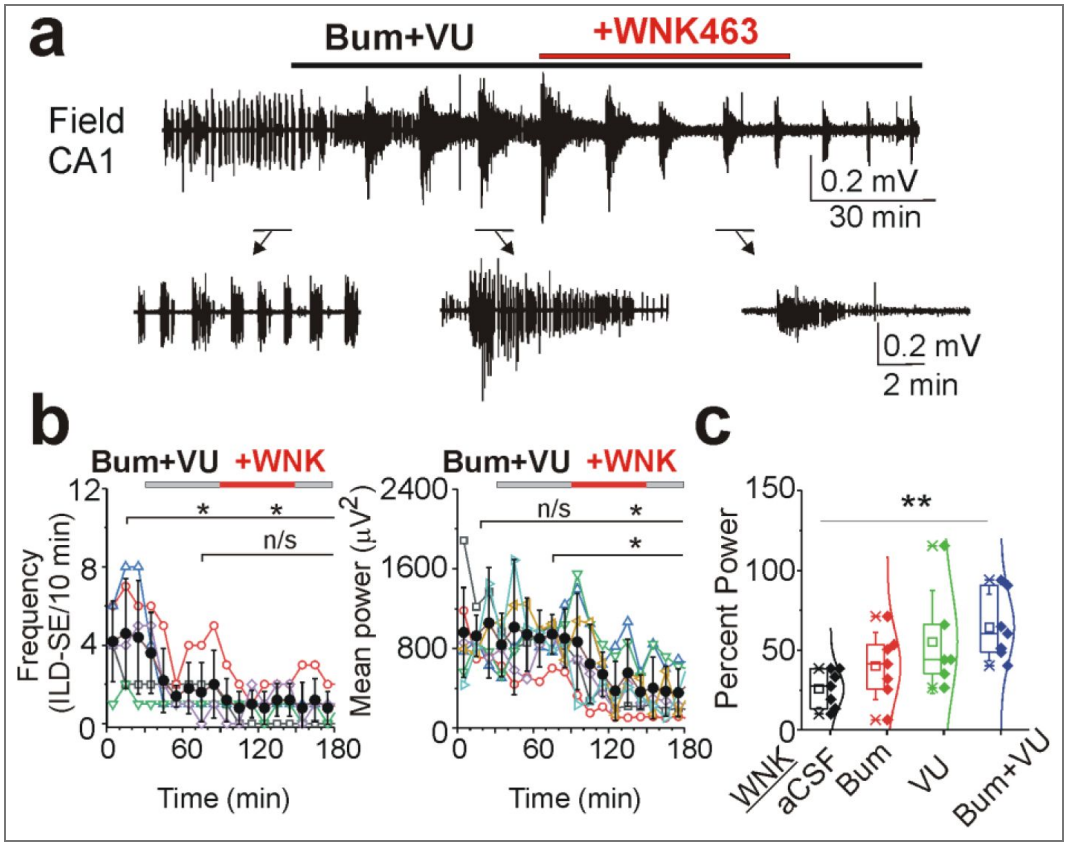

Figure 9. Simultaneous NKCC1 and KCC2 inhibition reduced the anti-ictal effects of WNK463.

(**a**) Extracellular field potential recordings in the CA1 pyramidal cell layer in the organotypic hippocampal slices *in vitro*. WNK463 (1 μM) was applied in the presence of NKCC1 and KCC2 blockers bumetanide (10 μM) and VU0463271 (1 μM). Expansion of recurrent ILDs before and during drug applications. (**b**) WNK463 application in the presence of bumetanide in composition with VU0463271 did not change the frequency of ILDs but significantly reduced the mean power of epileptiform discharges preceding WNK463 application (*p<0.05; One-Way RM ANOVA, Tukey test). (**c**) Summary data of the effects of WNK463 on the mean power of electrical activity in control ACSF, in the presence of bumetanide (10 μM), in the presence of VU0463271 (1 μM), and in the composition of bumetanide (10 μM) and VU0463271 (1 μM). Simultaneous NKCC1 and KCC2 inhibition significantly reduced the anti-ictal effects of WNK463 (**P<0.01; One Way ANOVA, Holm-Sidak test).

Discussion

There is substantial interest in targeting the WNK-SPAK/OSR1-CCCs pathway for the therapy of various neurological disorders, including ischemic stroke (Josiah et al., 2021), neuropathic pain (Shekarabi et al., 2017), and anticonvulsant resistant seizures (Lee et al., 2022). We investigated the net effects of WNK463, an allosteric inhibitor of WNK-SPAK/OSR1 signaling, on $[Cl^-]_i$ elevation and extrusion rates during recurrent ILDs. We found that WNK463 improved $[Cl^-]_i$ homeostasis, progressively enhanced postictal $[Cl^-]_i$ extrusion rates, reduced ictal duration and abolished recurrent ILDs. Our pharmacological investigations suggest that the powerful anti-ictal effects of WNK463 are mediated by reduced NKCC1 and enhanced KCC2 transport activity that more efficiently prevent $[Cl^-]_i$ elevation and reduce activity-dependent increases in $[Cl^-]_i$ by suppression of ILDs.

Neuronal $[Cl^-]_i$ is a critical factor in determining whether postsynaptic $GABA_A$-R mediated signaling is inhibitory or excitatory. In pathological conditions such as brain trauma, cytotoxic edema and/or recurrent seizures, in which Cli may already be elevated, intense GABAergic input can further overwhelm the mechanisms that regulate chloride levels, leading to pathological increases in $[Cl^-]_i$ (Figures 1, 3-5). When $[Cl^-]_i$ increases, the E_{GABA} shifts towards more positive values, causing GABA-mediated depolarization and making neurons more likely to fire. This activity-dependent $[Cl^-]_i$ accumulation and a consequent shift from inhibitory to excitatory GABAergic signaling have been suggested to contribute to generation of ictal-like discharges (Fujiwara-Tsukamoto et al., 2006;Fujiwara-Tsukamoto et al., 2010;Ellender et al., 2014).

Restoration of $[Cl^-]_i$ equilibrium after synaptic activity is achieved by the net regulated activities of NKCC1 and KCC2 (Gamba, 2005). The NKCC1 membrane protein is the Na^+-K^+-$2Cl^-$ transporter that under physiological conditions facilitates the uptake of Cl^- into cells, playing a crucial role in regulation of cell volume and $[Cl^-]_i$, especially during early brain development. NKCC1 facilitates seizures in the developing brain and pharmacological inhibition of NKCC1 enhances the efficacy of GABAergic anticonvulsants (Dzhala et al., 2005;Dzhala et al., 2008;Soul et al., 2021).Increased NKCC1 levels have also been observed in the subiculum of temporal lobe epilepsy patients (Palma et al., 2006;Huberfeld et al., 2007) and in several models of epilepsy, such as those induced by a reactive astrogliosis (Robel et al., 2015) or traumatic brain injury (Wang et al., 2017).

The KCC2 protein is a potassium-chloride co-transporter that maintains low $[Cl^-]_i$ (Rivera et al., 1999). Reduced KCC2 function or expression can contribute to activity-dependent accumulations of chloride and the excitatory shift in GABA signaling. Previous studies demonstrated the role of KCC2 transport activity in extrusion of $[Cl^-]_i$ and termination of ILDs (Sivakumaran et al., 2015;Dzhala and Staley, 2021). Our current data confirm that the high-affinity KCC2 inhibitor VU0463271 increased $[Cl^-]_i$ elevation and the duration of ILDs suggesting that inadequate KCC2 function contributes to the transition from the short ictal-like events to sustained *status epilepticus* (Figure 7). In contrast, activation of KCC2 transport activity efficiently recovers E_{Cl} during ILDs and restores GABAergic inhibition. These effects were correlated with more rapid termination of ILDs and electrical *status epilepticus* (Dzhala and Staley, 2021;Jarvis et al., 2023).

Hypoxia-ischemia, acute brain trauma, and recurrent seizures alter the equilibrium value of Cl^- and impair the functional regulation of the CCCs, and are associated with cytotoxic cell swelling, acute and chronic accumulation of $[Cl^-]_i$, and GABA depolarizing responses, which foster seizures and anticonvulsant resistance via failure of inhibition (Dzhala et al., 2010;Dzhala et al., 2012). Antagonizing NKCC1 activity and/or stimulating KCC2 activity might reduce swelling and $[Cl^-]_i$ in injured neurons, restore GABAergic inhibition, suppress seizures, and prevent epileptogenesis.

NKCC1 and KCC2 are rapidly stimulated and inhibited, respectively, by direct phosphorylation mediated by the Cl^--sensitive WNK-SPAK/OSR1 complex (Alessi et al., 2014). The WNK family senses changes in the $[Cl^-]_i$, cell volume, extracellular osmolarity and transduces this information to CCCs (Shekarabi et al., 2017). WNKs stimulate the kinases SPAK and OSR1, which directly phosphorylate and stimulate NKCC1 or inhibit KCC2 (Kahle et al., 2013). Conversely, inhibiting the WNK-SPAK/OSR1 pathway might be an especially potent strategy to reduce neuronal Cl^-

elevation and facilitate neuronal Cl^- extrusion by coincident NKCC1 inhibition and KCC2 activation. It was demonstrated that promoting KCC2 activity via WNK-SPAK/OSR1 inhibition can improve GABAergic inhibition and reduce neuronal excitability, potentially mitigating seizure activity (Lee et al., 2022).

Confusion may arise when discussing "baseline $[Cl^-]_i$" (Lee et al., 2022). In the presence of TTX, there is minimal synaptic GABA-mediated Cl^- loading, and the measured $[Cl^-]_i$ is the baseline $[Cl^-]_i$. During recurrent seizure activity, the $[Cl^-]_i$ measured between seizures is not likely to be at baseline due to ictal cytoplasmic Cl^- loading from GABA-mediated synaptic influx and incomplete cotransport of the excess $[Cl^-]_i$ out of the neuron. In this study, we found that the rate of Cl^- transport out of the neuron was enhanced by blocking the WNK-SPAK/OSR1 pathway. Blocking this pathway did not change baseline $[Cl^-]_i$ significantly. However, blocking this pathway did reduce the interictal $[Cl^-]_i$ by enhancing the export of the ictal GABA-mediated Cl^- load. Considered from the point of Michaelis-Menten kinetics, changing the maximum velocity of Cl^-cotransport does not alter the affinity of the transporter for $[Cl^-]_i$, which from this point of view would affect baseline $[Cl^-]_i$ (Staley and Proctor, 1999). Considered from the view baseline $[Cl^-]_i$ being set by Donnan exclusion (Glykys et al., 2014;Rahmati et al., 2021;Staley, 2024), altering the maximum velocity of Cl^- cotransport would also not be expected to alter baseline $[Cl^-]_i$.

Limitations and future directions

Our experiments were conducted *in vitro*. This provides excellent control of the extracellular environment and imaging but does not replicate the *in vivo* vascular supply and maintenance of ionic homeostasis. While we find that increased WNK-SPAK/OSR1-mediated KCC2 activity via enhanced Cl^- extrusion rates robustly reduces seizure activity *in vitro*, it is possible that *in vivo*, increased KCC2 activity could lead to extracellular potassium accumulations (Viitanen et al., 2010) that would limit Cl^- extrusion independently of the velocity of KCC2 transport (Thompson et al., 1988;Staley and Proctor, 1999). Thus, it will be important to assess these findings *in vivo*.

Materials and Methods

All animal-use protocols were in accordance with the guidelines of the National Institute of Health and the Massachusetts General Hospital Center for Comparative Medicine on the use of laboratory animals. All protocols were approved by the MGH Institutional Animal Care and Use Committee (IACUC).

Culture of Organotypic Hippocampal Slices and Experimental Conditions

Transverse 350 μm hippocampal slices were prepared from C57BL/6, Clm1 (Duke University Medical Center, Durham, NC, USA) and sClm mice of either sex at postnatal (P) day 6-7 as previously described (Dyhrfjeld-Johnsen et al., 2010;Berdichevsky et al., 2012). Acute slices were mounted on poly-L-Lysine coated glass coverslips (Electron Microscopy Sciences, Hatfield, PA). Slices were incubated in 1000 μL of NeuroBasal/B27(1X) medium (Gibco by Life Technologies, Grant Island, NY) supplemented with 0.5 mM GlutaMAX and 30 μg/mL gentamicin (all from Invitrogen, Carlsbad, CA) in 6-well plates with low-evaporation lid (Becton Dickinson Labware, Franklin Lakes, NJ), in a humidified 37°C atmosphere that contained 5% CO_2, placed on a rocking platform (< 1 cycle/min). Culture medium was changed bi-weekly. For acute recordings and imaging, slices were transferred to a submerged chamber and continuously superfused in oxygenated (95% O_2 and 5% CO_2) artificial cerebrospinal fluid (ACSF) containing (in mM): 126 NaCl, 3.5 KCl, 2 $CaCl_2$, 1.3 $MgCl_2$, 25 $NaHCO_3$, 1.2 $NaHPO_4$ and 11 Glucose (pH 7.4) at 32 ± 0.5°C and a flow rate of 2 mL/min. All organotypic hippocampal slices were used at Day *in Vitro* (DIV) 9-21.

Pharmacological agents included bumetanide at a low concentration (10 μM) that blocks NKCC1, bumetanide at a high concentration (500 μM) that blocks NKCC1 and KCCs, the specific KCC2 blocker VU0463271 (1 μM), the $GABA_A$ receptor ($GABA_A$-R) antagonist SR95531 (10 μM), and the sodium voltage gated channel antagonist Tetrodotoxin (1 μM). Bumetanide and SR95531 were

from Sigma-Aldrich CO, St. Louis, MO. VU0463271 and TTX were from TOCRIS Bioscience, Bristol, UK. WNK463 (1 μM) was from MedChemExpress, Monmouth Junction, NJ. Dimethyl sulfoxide (DMSO; 100 μl/100 ml) was used as an organic solvent (Dzhala and Staley, 2021).

siRNA targeted genetic silencing of NKCC1 and KCC2

NKCC1 and KCC2 were selectively silenced using Dharmacom Accell™ (Dharmacon, Inc., Lafayette, CO) siRNA reagents in organotypic hippocampal brain slices at DIV 9-14. This siRNA technology does not require transfection reagents or instrument-based procedures that may result in loss of cell viability. Synthetic RNAi reagents were resuspended in RNAase-free solution (1x siRNA buffer diluted from 5x siRNA buffer (Item # B-002000-UB-100) using molecular grade RNAase-free water (Item # B-003000-WB-100)) according to siRNA resuspension protocol. Resuspended siRNA reagents were mixed with Accell delivery media (Item # B-005000-100) and used immediately. The final concentration was 1 μM siRNA per well in a 6-well plate. Culture medium was replaced with 1000 μL of the appropriate delivery mix (Accell siRNA and delivery media) to each well. Starting from DIV8-9, the organotypic slices were incubated in Accell siRNA delivery media at 37°C with 5% CO_2 for 72 hours. As indicated by assay-dependent requirements (such as knockdown detection of a long-lived protein), Accell siRNA delivery media was changed back to culture medium and incubated at 37°C with 5% CO_2 for an additional 24-72 hours following the standard 72 hours Accell incubation prior to assessing electrophysiological recordings and/or protein knockdown. Target sequence for ON-TARGET plus mouse Slc12a2 (NKCC1) siRNA (Item # L-044448-01-0020) was: (1) ACUAAGACAUAUCGACAGA, (2) CUAUGUAUGUUGUCGGAUU, (3) GAUUGUAAGAUCCGAGUAU, (4) AGGUCAAGCAAGACGUUAA; for mouse Slc12a5 (KCC2) siRNA (Item # L-058596-01-0020): (1) CGGCAUACACCUACGAGAA, (2) CAGGAGACAUCGCGUGUAU, (3) GAGCAAAGUUUCCGUUGAU, (4) UGGAGAUGCAUGAGAGCGA. Accell non-targeting siRNA (Item # D-001920-02-05) and Accell green (fluorescein) non-targeting siRNA (Item # D-001950-01-05) were used for control and siRNA delivery visualization.

Immunohistochemistry and confocal imaging were used for verification of siRNA targeted gene silencing (Bahari et al., 2024). Organotypic slices were prepared and processed for sequential immunostaining using a modified version of the protocol previously described in (Gogolla et al., 2006). The incubation time with primary antibody was extended to 3 nights, and 20% BSA in PBS was used as a blocking solution. The rabbit monoclonal anti-NKCC1 (1:200; AB303518-1007, lot # 1129040-4 from Abcam Inc, Waltham, MA) and mouse monoclonal anti-KCC2 (1:200; MABN88, lot # 4315985 from Millipore Sigma, Temecula, CA) were used as primary antibodies. The goat anti-rabbit Alexa Fluor 488 and goat anti-mouse Alexa Fluor 594 (1:1000; all from Invitrogen by ThermoFisher Scientific, Eugene, Oregon) were used as secondary antibodies.

Slices were washed and mounted onto glass microscope slides and covered by coverslip glass and mounting medium (Fluoromount-G, with DAPI, Invitrogen by ThermoFisher Scientific). Images were acquired on an Olympus FLUOVIEW FV3000 confocal laser scanning microscope and analyzed using ImageJ 1.53k software (Wayne Rasband and contributors, National Institutes of Health, USA). NKCC1 and KCC2 immunoreactivity (IR) were quantified within DG and CA1 regions of interest (ROIs). For each ROI, NKCC1 or KCC2 IR-positive area was normalized to the DAPI-positive area within the same region. Images were blinded, and a threshold for IR was determined across all images for each antibody. NKCC1-, KCC2-, and DAPI-positive areas were measured using the “Measure” function in ImageJ. Normalized IR was calculated as the NKCC1- or KCC2-positive area divided by the DAPI-positive area within the same DG or CA1 ROI.

Electrophysiological recordings and data analysis

Extracellular field potentials were recorded in the CA3 and CA1 pyramidal cell layer of organotypic hippocampal slices using custom-made tungsten-coated 50 μm wire microelectrodes and ISO-DAM8A amplifier (WPI, Sarasota, FL). The electrical signals were digitized using an analog-to-digital converter DigiData 1322A (Axon Instruments, Inc, Union City, CA). AxoScope 10.7 and Clampfit 10.7 (Molecular Devices, San Jose, CA), Origin 2018 (OriginLab Corporation, Northampton, MA) and SigmaPlot 11.0 (Systat Software, Inc, San Jose, CA) programs were used for

data acquisition and analyses. Recordings were sampled at 10 kHz. Interictal epileptiform discharges (IEDs) were defined as synchronous network-driven bursts characterized by short (0.1-3 s) duration and large amplitude population spikes. The frequency, duration, and amplitude of IEDs substantially varied between recurrent ictal-like discharges. Ictal-like discharges (ILDs) were defined as hyper-synchronous, large-amplitude and high-frequency population spikes followed by sustained ictal-tonic and/or intermittent ictal-clonic after-discharges, with the duration of the population spikes and after-discharge complex lasting more than 5 seconds, and subsequent post-ictal depression. *Status epilepticus* was defined as continuous ILDs for at least 5 min, or by sustained ictal-like tonic-clonic epileptiform discharges without recovery to baseline activity between the ILDs. Power spectrum analysis was performed on the electrical recordings after filtering with a Bessel high pass filter of 1Hz and applying a Hamming window function. The power of the electrical activity was calculated by integrating the root mean square value of the signal amplitude in corresponding time windows and frequency range from 1 to 1000 Hz. For comparison between slices, power was normalized for each slice with the highest value in control conditions.

Two-photon imaging of Clomeleon, quantitative and morphological analysis

Neuronal chloride concentration was determined in CA1 pyramidal neurons expressing the ratiometric chloride indicators Clomeleon (Clm) (Kuner and Augustine, 2000) and superClomeleon (sClm) (Grimley et al., 2013; Rahmati et al., 2021). High-resolution two-photon excitation laser scanning imaging of the Cl^--sensitive yellow fluorescent protein (YFP) and the Cl^--insensitive cyan fluorescent protein (CFP) was performed on an Olympus Fluoview 1000 MPE microscope. A mode-locked titanium-sapphire laser (MaiTai, Spectra Physics) with 860 nm two-photon excitation was used to generate fluorescence. Emitted light passed through a dichroic mirror and was band-pass filtered through 480±15 nm (D480/30) for CFP and a 535±20 nm filter (D535/40) for YFP (FV10-MRCYR/XR). Time series acquisition of 720 frames (256x256 pixels for 254.46x254.46 µm) with 5-10 second intervals was performed to measure chloride concentration as a function of time in control conditions, during a 30-60 min period of applications of drugs, and over a 30-60 min period of wash-out. Transition from 10% above interictal $[Cl^-]_i$ to 90% of its maximal amplitude during onset of ILDs was used to estimate $[Cl^-]_i$ rise time. Mono-exponential fit (y=y0+A1*exp(–(x– x0)/t1) was used to estimate the decay time constant (t1) of $[Cl^-]_i$ recovery to baseline in individual cells.

For morphological analysis, organotypic slices were imaged through the CA1 pyramidal cell layer (Z-axis dimension 0-100 µm, 1-2 µm step size). ImageJ 1.51 software (National Institutes of Health) was used for quantitative analysis. Region of interests (ROIs) were selected using the chloride insensitive CFP fluorescence. The ratio of the YFP/CFP fluorescence intensity was used for $[Cl^-]_i$ calculation (Kuner and Augustine, 2000;Berglund et al., 2008;Glykys et al., 2009). The CFP emission of Clomeleon was used for the high-resolution morphological analysis (Dzhala et al., 2012).

Statistical analysis

Group measures are expressed as mean ± standard deviation (SD) or median (25%-75%) ± SD as indicated. The Shapiro-Wilk test was used to determine normality of the data. The Student's *t* test (paired or unpaired) was performed for parametric comparison of normally distributed data. The Wilcoxon Signed Rank Test (paired data), and Mann-Whitney test (unpaired data, two-tail) were used for non-parametric comparison of arbitrary distributed data. One-way repeated measures analysis of variance (One Way RM ANOVA) was used for multiple comparison of parametric data to evaluate the differences in the mean values among the control and treatment groups. The Friedman RM ANOVA on Ranks was used for non-parametric data to determine the differences in the median values among the control and treatment groups. In a One Way RM ANOVA, (DF) represents the between-groups degree of freedom. In the Friedman RM ANOVA on Ranks, the chi-square statistic was used to assess the differences between the groups. The Tukey Test or Holm-Sidak Test was used for all pairwise comparisons of the responses to the different treatment

groups. In the Tukey or Holm-Sidak test, (df) refers to the difference of means in the ANOVA, and (dr) refers to the difference of ranks in the ANOVA on Ranks. The level of significance was set at $P<0.05$.

Data availability

All data generated and analyzed during this study are included in the manuscript.

Acknowledgements

The authors acknowledge funding from the National Institutes of Health and National Institute of Neurological Disorders and Stroke grant R01NS120973 to VID and R35NS116852 to KJS.

Additional information

Author contributions

DV - Conceptualization, Formal analysis, Validation, Investigation, Visualization, Methodology, Writing—original draft, Project administration, Writing—review and editing.

FHS, NR, AC, RB - Formal analysis, Validation, Investigation, Visualization, Methodology.

KK, KS - Conceptualization, Resources, Supervision, Funding acquisition, Project administration, Writing—review and editing.

Ethics

Animal experimentation: All animal experimental procedures were performed in accordance with the National Institutes of Health Guide for the Care and Use of Laboratory Animals and approved by the MGH Institutional Animal Care and Use Committee (IACUC Protocol# 2020N000213).

Funding

This paper was supported by the following grants:

NIH and NINDS R01NS120973 to Volodymyr I Dzhala, NIH and NINDS R35NS116852 to Kevin J Staley

The funders had no role in study design, data collection and interpretation, or the decision to submit the work for publication.

Funding

Funder	Grant reference number	Author
HHS | NIH | National Institute of Neurological Disorders and Stroke (NINDS)	R01NS120973	Volodymyr I Dzhala
HHS | NIH | National Institute of Neurological Disorders and Stroke (NINDS)	R35NS116852	Kevin Staley

Author ORCID iDs

Volodymyr I Dzhala: https://orcid.org/0009-0001-2875-4352

References

Alessi DR, Zhang J, Khanna A, Hochdorfer T, Shang Y, Kahle KT (2014) The WNK-SPAK/OSR1 pathway: master regulator of cation-chloride cotransporters. *Sci Signal* **7**:re3 https://doi.org/10.1126/scisignal.2005365 | PubMed

Andreasen M, Nedergaard S (2017) Furosemide depresses the presynaptic fiber volley and modifies frequency-dependent axonal excitability in rat hippocampus. *J Neurophysiol* **117**:1512-1523 https://doi.org/10.1152/jn.00704.2016 | PubMed

Bahari F, Dzhala V, Balena T, Lillis KP, Staley KJ (2024) Intraventricular haemorrhage in premature infants: the role of immature neuronal salt and water transport. *Brain* **147**:3216-3233 https://doi.org/10.1093/brain/awae161 | PubMed

Berdichevsky Y, Dzhala V, Mail M, Staley KJ (2012) Interictal spikes, seizures and ictal cell death are not necessary for post-traumatic epileptogenesis in vitro. *Neurobiol Dis* **45**:774-785 https://doi.org/10.1016/j.nbd.2011.11.001 | PubMed

Berglund K, Schleich W, Wang H, Feng G, Hall WC, Kuner T, Augustine GJ (2008) Imaging synaptic inhibition throughout the brain via genetically targeted Clomeleon. *Brain Cell Biol* **36**:101-118 https://doi.org/10.1007/s11068-008-9031-x | PubMed

Blaesse P, Airaksinen MS, Rivera C, Kaila K (2009) Cation-chloride cotransporters and neuronal function. *Neuron* **61**:820-838 https://doi.org/10.1016/j.neuron.2009.03.003 | PubMed

Cleary RT, Sun H, Huynh T, Manning SM, Li Y, Rotenberg A, Talos DM, Kahle KT, Jackson M, Rakhade SN, *et al.* (2013) Bumetanide enhances phenobarbital efficacy in a rat model of hypoxic neonatal seizures. *PLoS One* **8**:e57148 https://doi.org/10.1371/journal.pone.0057148 | PubMed

Côme E, Blachier S, Gouhier J, Russeau M, Levi S (2023) Lateral Diffusion of NKCC1 Contributes to Chloride Homeostasis in Neurons and Is Rapidly Regulated by the WNK Signaling Pathway. *Cells* **12**:464 https://doi.org/10.3390/cells12030464 | PubMed

de Los HP, Alessi DR, Gourlay R, Campbell DG, Deak M, Macartney TJ, Kahle KT, Zhang J (2014) The WNK-regulated SPAK/OSR1 kinases directly phosphorylate and inhibit the K+-Cl- co-transporters. *Biochem J* **458**:559-573 https://doi.org/10.1042/bj20131478 | PubMed

Dyhrfjeld-Johnsen J, Berdichevsky Y, Swiercz W, Sabolek H, Staley KJ (2010) Interictal spikes precede ictal discharges in an organotypic hippocampal slice culture model of epileptogenesis. *J Clin Neurophysiol* **27**:418-424 https://doi.org/10.1097/wnp.0b013e3181fe0709 | PubMed

Dzhala V, Staley KJ (2015) Acute and chronic efficacy of bumetanide in an in vitro model of posttraumatic epileptogenesis. *CNS Neurosci Ther* **21**:173-180 https://doi.org/10.1111/cns.12369 | PubMed

Dzhala V, Valeeva G, Glykys J, Khazipov R, Staley K (2012) Traumatic alterations in GABA signaling disrupt hippocampal network activity in the developing brain. *J Neurosci* **32**:4017-4031 https://doi.org/10.1523/jneurosci.5139-11.2012 | PubMed

Dzhala VI, Brumback AC, Staley KJ (2008) Bumetanide enhances phenobarbital efficacy in a neonatal seizure model. *Ann Neurol* **63**:222-235 https://doi.org/10.1002/ana.21229 | PubMed

Dzhala VI, Kuchibhotla KV, Glykys JC, Kahle KT, Swiercz WB, Feng G, Kuner T, Augustine GJ, Bacskai BJ, Staley KJ (2010) Progressive NKCC1-dependent neuronal chloride accumulation during neonatal seizures. *J Neurosci* **30**:11745-11761 https://doi.org/10.1523/jneurosci.1769-10.2010 | PubMed

Dzhala VI, Mail M, Staley KJ (2024) Timing of interventions to control neuronal chloride elevation in a model of neonatal seizures after hippocampal injury. *Epilepsia* **65**:3391-3405 https://doi.org/10.1111/epi.18108 | PubMed

Dzhala VI, Staley KJ (2003) Excitatory Actions of Endogenously Released GABA Contribute to Initiation of Ictal Epileptiform Activity in the Developing Hippocampus. *J Neurosci* **23**:1840-1846 https://doi.org/10.1523/jneurosci.23-05-01840.2003 | PubMed

Dzhala VI, Staley KJ (2021) KCC2 Chloride Transport Contributes to the Termination of Ictal Epileptiform Activity. *eNeuro* **8**:ENEURO.0208-20.2020 https://doi.org/10.1523/eneuro.0208-20.2020 | PubMed

Dzhala VI, Talos DM, Sdrulla DA, Brumback AC, Mathews GC, Benke TA, Delpire E, Jensen FE, Staley KJ (2005) NKCC1 transporter facilitates seizures in the developing brain. *Nat Med* **11**:1205-1213 https://doi.org/10.1038/nm1301 | PubMed

Ellender TJ, Raimondo JV, Irkle A, Lamsa KP, Akerman CJ (2014) Excitatory effects of parvalbumin-expressing interneurons maintain hippocampal epileptiform activity via synchronous afterdischarges. *J Neurosci* **34**:15208-15222 https://doi.org/10.1523/jneurosci.1747-14.2014 |

PubMed

Fujiwara-Tsukamoto Y, Isomura Y, Imanishi M, Ninomiya T, Tsukada M, Yanagawa Y, Fukai T, Takada M (2010) Prototypic seizure activity driven by mature hippocampal fast-spiking interneurons. *J Neurosci* **30**:13679-13689 https://doi.org/10.1523/jneurosci.1523-10.2010 | PubMed

Fujiwara-Tsukamoto Y, Isomura Y, Takada M (2006) Comparable GABAergic mechanisms of hippocampal seizurelike activity in posttetanic and low-Mg2+ conditions. *J Neurophysiol* **95**:2013-2019 https://doi.org/10.1152/jn.00238.2005 | PubMed

Gagnon M, Bergeron MJ, Lavertu G, Castonguay A, Tripathy S, Bonin RP, Perez-Sanchez J, Boudreau D, Wang B, Dumas L, *et al.* (2013) Chloride extrusion enhancers as novel therapeutics for neurological diseases. *Nat Med* **19**:1524-1528 https://doi.org/10.1038/nm.3356 | PubMed

Gamba G (2005) Molecular physiology and pathophysiology of electroneutral cation-chloride cotransporters. *Physiol Rev* **85**:423-493 https://doi.org/10.1152/physrev.00011.2004 | PubMed

Glykys J, Dzhala V, Egawa K, Balena T, Saponjian Y, Kuchibhotla KV, Bacskai BJ, Kahle KT, Zeuthen T, Staley KJ (2014) Local impermeant anions establish the neuronal chloride concentration. *Science* **343**:670-675 https://doi.org/10.1126/science.1245423 | PubMed

Glykys J, Dzhala V, Egawa K, Kahle KT, Delpire E, Staley K (2017) Chloride Dysregulation, Seizures, and Cerebral Edema: A Relationship with Therapeutic Potential. *Trends Neurosci* **40**:276-294 https://doi.org/10.1016/j.tins.2017.03.006 | PubMed

Glykys J, Dzhala VI, Kuchibhotla KV, Feng G, Kuner T, Augustine G, Bacskai BJ, Staley KJ (2009) Differences in cortical versus subcortical GABAergic signaling: a candidate mechanism of electroclinical uncoupling of neonatal seizures. *Neuron* **63**:657-672 https://doi.org/10.1016/j.neuron.2009.08.022 | PubMed

Gogolla N, Galimberti I, DePaola V, Caroni P (2006) Staining protocol for organotypic hippocampal slice cultures. *Nat Protoc* **1**:2452-2456 https://doi.org/10.1038/nprot.2006.180 | PubMed

Grimley JS, Li L, Wang W, Wen L, Beese LS, Hellinga HW, Augustine GJ (2013) Visualization of synaptic inhibition with an optogenetic sensor developed by cell-free protein engineering automation. *J Neurosci* **33**:16297-16309 https://doi.org/10.1523/jneurosci.4616-11.2013 | PubMed

Hochman DW, Baraban SC, Owens JW, Schwartzkroin PA (1995) Dissociation of synchronization and excitability in furosemide blockade of epileptiform activity. *Science* **270**:99-102 https://doi.org/10.1126/science.270.5233.99 | PubMed

Huberfeld G, Wittner L, Clemenceau S, Baulac M, Kaila K, Miles R, Rivera C (2007) Perturbed chloride homeostasis and GABAergic signaling in human temporal lobe epilepsy. *J Neurosci* **27**:9866-9873 https://doi.org/10.1523/jneurosci.2761-07.2007 | PubMed

Jarvis R, et al. (2023) Direct activation of KCC2 arrests benzodiazepine refractory status epilepticus and limits the subsequent neuronal injury in mice. *Cell Rep Med* **4**:100957 https://doi.org/10.1016/j.xcrm.2023.100957 | PubMed

Jedlicka P, Deller T, Gutkin BS, Backus KH (2011) Activity-dependent intracellular chloride accumulation and diffusion controls GABA(A) receptor-mediated synaptic transmission. *Hippocampus* **21**:885-898 https://doi.org/10.1002/hipo.20804 | PubMed

Josiah SS, Meor Azlan NF, Zhang J (2021) Targeting the WNK-SPAK/OSR1 Pathway and Cation-Chloride Cotransporters for the Therapy of Stroke. *Int J Mol Sci* **22**:1232 https://doi.org/10.3390/ijms22031232 | PubMed

Kahle KT, Deeb TZ, Puskarjov M, Silayeva L, Liang B, Kaila K, Moss SJ (2013) Modulation of neuronal activity by phosphorylation of the K-Cl cotransporter KCC2. *Trends Neurosci* **36**:726-737 https://doi.org/10.1016/j.tins.2013.08.006 | PubMed

Kahle KT, Rinehart J, Ring A, Gimenez I, Gamba G, Hebert SC, Lifton RP (2006) WNK protein kinases modulate cellular Cl- flux by altering the phosphorylation state of the Na-K-Cl and K-Cl cotransporters. *Physiology* **21**:326-335 https://doi.org/10.1152/physiol.00015.2006 | PubMed

Kahle KT, Staley KJ, Nahed BV, Gamba G, Hebert SC, Lifton RP, Mount DB (2008) Roles of the cation-chloride cotransporters in neurological disease. *Nat Clin Pract Neurol* **4**:490-503 https://doi.org/10.1038/ncpneuro0883 | PubMed

Khalilov I, Holmes GL, Ben-Ari Y (2003) In vitro formation of a secondary epileptogenic mirror focus by interhippocampal propagation of seizures. *Nat Neurosci* **6**:1079-1085 https://doi.org/10.1038/nn1125 | PubMed

Khazipov R, Khalilov I, Tyzio R, Morozova E, Ben Ari Y, Holmes GL (2004) Developmental changes in GABAergic actions and seizure susceptibility in the rat hippocampus. *Eur J Neurosci* **19**:590-600 https://doi.org/10.1111/j.0953-816x.2003.03152.x | PubMed

Kikuchi E, Mori T, Zeniya M, Isobe K, Ishigami-Yuasa M, Fujii S, Kagechika H, Ishihara T, Mizushima T, Sasaki S, *et al.* (2015) Discovery of Novel SPAK Inhibitors That Block WNK Kinase Signaling to Cation Chloride Transporters. *J Am Soc Nephrol* **26**:1525-1536 https://doi.org/10.1681/asn.2014060560 | PubMed

Korpi ER, Luddens H (1997) Furosemide interactions with brain GABAA receptors. *Br J Pharmacol* **120**:741-748 https://doi.org/10.1038/sj.bjp.0700922 | PubMed

Kuner T, Augustine GJ (2000) A genetically encoded ratiometric indicator for chloride: capturing chloride transients in cultured hippocampal neurons. *Neuron* **27**:447-459 https://doi.org/10.1016/s0896-6273(00)00056-8 | PubMed

Lee KL, Abiraman K, Lucaj C, Ollerhead TA, Brandon NJ, Deeb TZ, Maguire J, Moss SJ (2022) Inhibiting with-no-lysine kinases enhances K+/Cl- cotransporter 2 activity and limits status epilepticus. *Brain* **145**:950-963 https://doi.org/10.1093/brain/awab343 | PubMed

Liesemer K, Bratton SL, Zebrack CM, Brockmeyer D, Statler KD (2011) Early Post-Traumatic Seizures in Moderate to Severe Pediatric Traumatic Brain Injury: Rates, Risk Factors, and Clinical Features. *J Neurotrauma* **28**:755-762 https://doi.org/10.1089/neu.2010.1518 | PubMed

Lillis KP, Kramer MA, Mertz J, Staley KJ, White JA (2012) Pyramidal cells accumulate chloride at seizure onset. *Neurobiol Dis* **47**:358-366 https://doi.org/10.1016/j.nbd.2012.05.016 | PubMed

Melo Z, de Los HP, Cruz-Rangel S, Vazquez N, Bobadilla NA, Pasantes-Morales H, Alessi DR, Mercado A, Gamba G (2013) N-terminal serine dephosphorylation is required for KCC3 cotransporter full activation by cell swelling. *J Biol Chem* **288**:31468-31476 https://doi.org/10.1074/jbc.m113.475574 | PubMed

Moore YE, Deeb TZ, Chadchankar H, Brandon NJ, Moss SJ (2018) Potentiating KCC2 activity is sufficient to limit the onset and severity of seizures. *Proc Natl Acad Sci U S A* **115**:10166-10171 https://doi.org/10.1073/pnas.1810134115 | PubMed

Mori T, Kikuchi E, Watanabe Y, Fujii S, Ishigami-Yuasa M, Kagechika H, Sohara E, Rai T, Sasaki S, Uchida S (2013) Chemical library screening for WNK signalling inhibitors using fluorescence correlation spectroscopy. *Biochem J* **455**:339-345 https://doi.org/10.1042/bj20130597 | PubMed

Moriguchi T, Urushiyama S, Hisamoto N, Iemura S, Uchida S, Natsume T, Matsumoto K, Shibuya H (2005) WNK1 regulates phosphorylation of cation-chloride-coupled cotransporters via the STE20-related kinases, SPAK and OSR1. *J Biol Chem* **280**:42685-42693 https://doi.org/10.1074/jbc.m510042200 | PubMed

Mtchedlishvili Z, Kapur J (2006) High-affinity, slowly desensitizing GABAA receptors mediate tonic inhibition in hippocampal dentate granule cells. *Mol Pharmacol* **69**:564-575 https://doi.org/10.1124/mol.105.016683 | PubMed

Nardou R, Yamamoto S, Chazal G, Bhar A, Ferrand N, Dulac O, Ben-Ari Y, Khalilov I (2011) Neuronal chloride accumulation and excitatory GABA underlie aggravation of neonatal epileptiform activities by phenobarbital. *Brain* **134**:987-1002 https://doi.org/10.1093/brain/awr041 | PubMed

Palma E, Amici M, Sobrero F, Spinelli G, Di Angelantonio S, Ragozzino D, Mascia A, Scoppetta C, Esposito V, Miledi R, *et al.* (2006) Anomalous levels of Cl- transporters in the hippocampal subiculum from temporal lobe epilepsy patients make GABA excitatory. *Proc Natl Acad Sci U S A* **103**:8465-8468 https://doi.org/10.1073/pnas.0602979103 | PubMed

Payne JA (1997) Functional characterization of the neuronal-specific K-Cl cotransporter: implications for [K+]o regulation. *Am J Physiol* **273**:C1516-C1525 https://doi.org/10.1152/ajpcell.1997.273.5.c1516 | PubMed

Pisella LI, Gaiarsa JL, Diabira D, Zhang J, Khalilov I, Duan J, Kahle KT, Medina I (2019) Impaired regulation of KCC2 phosphorylation leads to neuronal network dysfunction and neurodevelopmental pathology. *Sci Signal* **12** https://doi.org/10.1126/scisignal.aay0300 | PubMed

Pond BB, Berglund K, Kuner T, Feng G, Augustine GJ, Schwartz-Bloom RD (2006) The chloride transporter Na(+)-K(+)-Cl- cotransporter isoform-1 contributes to intracellular chloride increases after in vitro ischemia. *J Neurosci* **26**:1396-1406 https://doi.org/10.1523/jneurosci.1421-05.2006 | PubMed

Rahmati N, Normoyle KP, Glykys J, Dzhala VI, Lillis KP, Kahle KT, Raiyyani R, Jacob T, Staley KJ (2021) Unique Actions of GABA Arising from Cytoplasmic Chloride Microdomains. *J Neurosci* **41**:4957-4975 https://doi.org/10.1523/jneurosci.3175-20.2021 | PubMed

Rivera C, Voipio J, Payne JA, Ruusuvuori E, Lahtinen H, Lamsa K, Pirvola U, Saarma M, Kaila K (1999) The K+/Cl- co-transporter KCC2 renders GABA hyperpolarizing during neuronal maturation. *Nature* **397**:251-255 https://doi.org/10.1038/16697 | PubMed

Robel S, Buckingham SC, Boni JL, Campbell SL, Danbolt NC, Riedemann T, Sutor B, Sontheimer H (2015) Reactive astrogliosis causes the development of spontaneous seizures. *J Neurosci* **35**:3330-3345 https://doi.org/10.1523/jneurosci.1574-14.2015 | PubMed

Roseth S, Fykse EM, Fonnum F (1995) Uptake of L-glutamate into rat brain synaptic vesicles: effect of inhibitors that bind specifically to the glutamate transporter. *J Neurochem* **65**:96-103 https://doi.org/10.1046/j.1471-4159.1995.65010096.x | PubMed

Shekarabi M, Zhang J, Khanna AR, Ellison DH, Delpire E, Kahle KT (2017) WNK Kinase Signaling in Ion Homeostasis and Human Disease. *Cell Metab* **25**:285-299 https://doi.org/10.1016/j.cmet.2017.01.007 | PubMed

Sigel E, Steinmann ME (2012) Structure, function, and modulation of GABA(A) receptors. *J Biol Chem* **287**:40224-40231 https://doi.org/10.1074/jbc.r112.386664 | PubMed

Sivakumaran S, Cardarelli RA, Maguire J, Kelley MR, Silayeva L, Morrow DH, Mukherjee J, Moore YE, Mather RJ, Duggan ME, *et al.* (2015) Selective inhibition of KCC2 leads to hyperexcitability and epileptiform discharges in hippocampal slices and in vivo. *J Neurosci* **35**:8291-8296 https://doi.org/10.1523/jneurosci.5205-14.2015 | PubMed

Sivakumaran S, Maguire J (2016) Bumetanide reduces seizure progression and the development of pharmacoresistant status epilepticus. *Epilepsia* **57**:222-232 https://doi.org/10.1111/epi.13270 | PubMed

Soul JS, Bergin AM, Stopp C, Hayes B, Singh A, Fortuno CR, O'Reilly D, Krishnamoorthy K, Jensen FE, Rofeberg V, *et al.* (2021) A pilot randomized, controlled, double-blind trial of bumetanide to treat neonatal seizures Controlled bumetanide trial for neonatal seizures. *Ann Neurol* **89**:327-340 https://doi.org/10.1002/ana.25959 | PubMed

Staley KJ (2024) Ionic Mechanisms of Ictogenic Disinhibition: All GABA Signaling Is Local. In: Noebels JL, Avoli M, Rogawski MA, et al (Eds). *Jasper's Basic Mechanisms of the Epilepsies* pp. 1467-1488

Staley KJ, Longacher M, Bains JS, Yee A (1998) Presynaptic modulation of CA3 network activity. *Nat Neurosci* **1**:201-209 https://doi.org/10.1038/651 | PubMed

Staley KJ, Proctor WR (1999) Modulation of mammalian dendritic GABA(A) receptor function by the kinetics of Cl- and HCO3 transport. *J Physiol* **519**:693-712 https://doi.org/10.1111/j.1469-7793.1999.0693n.x | PubMed

Steffensen AB, Sword J, Croom D, Kirov SA, MacAulay N (2015) Chloride Cotransporters as a Molecular Mechanism underlying Spreading Depolarization-Induced Dendritic Beading. *J Neurosci* **35**:12172-12187 https://doi.org/10.1523/jneurosci.0400-15.2015 | PubMed

Thompson SM, Deisz RA, Prince DA (1988) Relative contributions of passive equilibrium and active transport to the distribution of chloride in mammalian cortical neurons. *J Neurophysiol* **60**:105-124 https://doi.org/10.1152/jn.1988.60.1.105 | PubMed

van den Pol AN, Obrietan K, Chen G (1996) Excitatory actions of GABA after neuronal trauma. *J Neurosci* **16**:4283-4292 https://doi.org/10.1523/jneurosci.16-13-04283.1996 | PubMed

Van Harreveld A, Schade JP (1959) Chloride movements in cerebral cortex after circulatory arrest and during spreading depression. *J Cell Comp Physiol* **54**:65-84 https://doi.org/10.1002/jcp.1030540108 | PubMed

Viitanen T, Ruusuvuori E, Kaila K, Voipio J (2010) The K+-Cl cotransporter KCC2 promotes GABAergic excitation in the mature rat hippocampus. *J Physiol* **588**:1527-1540 https://doi.org/10.1113/jphysiol.2009.181826 | PubMed

Vitari AC, Thastrup J, Rafiqi FH, Deak M, Morrice NA, Karlsson HK, Alessi DR (2006) Functional interactions of the SPAK/OSR1 kinases with their upstream activator WNK1 and downstream substrate NKCC1. *Biochem J* **397**:223-231 https://doi.org/10.1042/bj20060220 | PubMed

Wang F, Wang X, Shapiro LA, Cotrina ML, Liu W, Wang EW, Gu S, Wang W, He X, Nedergaard M, *et al.* (2017) NKCC1 up-regulation contributes to early post-traumatic seizures and increased post-traumatic seizure susceptibility. *Brain Struct Funct* **222**:1543-1556 https://doi.org/10.1007/s00429-016-1292-z | PubMed

Watanabe M, Zhang J, Mansuri MS, Duan J, Karimy JK, Delpire E, Alper SL, Lifton RP, Fukuda A, Kahle KT (2019) Developmentally regulated KCC2 phosphorylation is essential for dynamic GABA-mediated inhibition and survival. *Sci Signal* **12** https://doi.org/10.1126/scisignal.aaw9315 | PubMed

Yamada K, et al. (2017) Optimization of Allosteric With-No-Lysine (WNK) Kinase Inhibitors and Efficacy in Rodent Hypertension Models. *J Med Chem* **60**:7099-7107 https://doi.org/10.1021/acs.jmedchem.7b00708 | PubMed

Zhang J, Karimy JK, Delpire E, Kahle KT (2017) Pharmacological targeting of SPAK kinase in disorders of impaired epithelial transport. *Expert Opin Ther Targets* **21**:795-804 https://doi.org/10.1080/14728222.2017.1351949 | PubMed

Peer reviews

Reviewer #1 (Public review):

Summary:

The authors used extracellular field potential recordings and two-photon imaging to monitor neuronal network activity and intracellular chloride concentration ([Cl-]i) in organotypic hippocampal slices from mice expressing the genetically encoded chloride fluorophore Clomeleon. These slices were used as a model of acute traumatic brain injury and epileptogenesis in vitro. The study provides evidence that blocking the WNK-SPAK/OSR1 pathway with WNK463 alleviates epileptic activity, and that this anticonvulsant effect involves suppression of the chloride loader NKCC1 and enhancement of chloride extrusion via KCC2. Overall, this is a solid study with a comprehensive pharmacological analysis.

Strengths:

The conclusions are well supported by the detailed pharmacological analysis.

Weaknesses:

The only weakness I see is the absence of cellular-level electrophysiology, which precludes interpretation of the imaging data in the context of GABA action polarity.

https://doi.org/10.7554/eLife.112181.1.sa2

Reviewer #2 (Public review):

Summary:

The authors investigate whether inhibition of the WNK-SPAK/OSR1 pathway using the allosteric inhibitor WNK463 improves neuronal chloride homeostasis and suppresses epileptiform activity in organotypic hippocampal slice cultures. Using Super Clomeleon imaging combined with extracellular field recordings, they demonstrate that WNK463 accelerates recovery of intracellular chloride following chloride loading, reduces interictal chloride accumulation, and progressively suppresses recurrent ictal-like discharges. Pharmacological inhibition and siRNA-mediated knockdown of NKCC1 and KCC2 are then used to investigate the contribution of these transporters to the anti-ictal effects of WNK463.

Strengths:

The study addresses an important question in the field of chloride homeostasis and epilepsy and combines complementary experimental approaches. In particular, the distinction between baseline chloride measured in the presence of TTX and activity-dependent interictal chloride accumulation provides a useful conceptual framework for interpreting previous studies of WNK-SPAK inhibition. The imaging, electrophysiological, and pharmacological data are internally consistent and support the conclusion that WNK463 alters chloride dynamics and substantially suppresses ictal-like activity in this model.

Weaknesses:

The principal limitation of the manuscript is that several mechanistic conclusions extend beyond the experimental observations. Throughout the results and discussion, the authors interpret the observed changes in intracellular chloride dynamics as evidence of enhanced CCC-mediated chloride extrusion, while the pharmacological and siRNA-mediated experiments are interpreted as supporting coordinated NKCC1 inhibition and KCC2 activation, ultimately leading to restoration of GABAergic inhibition and negative shifts in EGABA. While these interpretations are plausible and consistent with the data, they remain inferential because transporter phosphorylation or activity, EGABA, and inhibitory synaptic function were not directly assessed in the current study. Moreover, although the pharmacological and knockdown experiments support a contribution of NKCC1 and KCC2 to the actions of WNK463, they do not definitively establish coordinated modulation of both transporters as the primary mechanism underlying seizure suppression. These mechanistic conclusions should therefore be presented more cautiously.

The manuscript would also benefit from broader contextualization within the current literature. The introduction largely focuses on previous work from the authors' group and provides a relatively narrow overview of chloride homeostasis in epilepsy. In particular, the discussion would benefit from broader consideration of studies examining KCC2 dysfunction in human epilepsy and experimental models, alternative mechanisms regulating KCC2 activity following seizures, and recent therapeutic strategies targeting KCC2.

Finally, although the authors appropriately acknowledge that the experiments were performed exclusively in vitro, the discussion could more explicitly address the limitations of the organotypic hippocampal slice model, including how culture-induced network reorganization and spontaneous epileptiform activity may influence chloride homeostasis and the extent to which these findings generalize to traumatic brain injury and chronic epilepsy in vivo. In addition, the statistical analysis would benefit from clarification regarding the experimental unit and the treatment of repeated measurements.

https://doi.org/10.7554/eLife.112181.1.sa1

Reviewer #3 (Public review):

Summary:

Dzhala and colleagues present findings from organotypic slice cultures suggesting that simultaneous modulation of the complementary cation-chloride cotransporters NKCC1 and KCC2 through inhibition of the WNK-SPAK/OSR1 pathway reduces seizure-like activity. The manuscript is generally well written, and the data support the conclusion that WNK463 exerts robust anti-ictal effects in this model. However, several issues should be addressed to strengthen the mechanistic interpretation and statistical rigor of the study, and improve confidence in the conclusions.

Strengths:

(1) The study addresses an important mechanistic question by investigating how inhibition of the WNK-SPAK/OSR1 pathway with WNK463 influences seizure activity and neuronal chloride homeostasis.

(2) The experimental design is logical and comprehensive, progressing from characterization of chloride dynamics to pharmacological and genetic interrogation of the underlying mechanism using multiple complementary approaches, including pharmacological inhibition, siRNA-mediated knockdown, electrophysiology, and chloride imaging.

(3) The combination of simultaneous extracellular electrophysiology and two-photon chloride imaging provides complementary functional and mechanistic information and represents a major technical strength of the study.

(4) The TTX experiments elegantly distinguish activity-dependent chloride accumulation from resting intracellular chloride concentration, substantially strengthening the central mechanistic conclusions.

Weaknesses:

(1) The mechanistic conclusions regarding KCC2 activation and NKCC1 inhibition are stronger than the data directly support. Throughout the manuscript, the authors conclude that WNK463 activates KCC2 and inhibits NKCC1. Although this interpretation is consistent with the established biology of the WNK-SPAK/OSR1 pathway, the evidence presented here is indirect. Specifically, the authors infer KCC2 activation and NKCC1 inhibition from the observation that pharmacological inhibition or siRNA-mediated knockdown of these transporters alters the effects of WNK463, together with measurements of chloride dynamics. While these findings are compatible with a KCC2- and NKCC1-dependent mechanism, they do not directly establish that WNK463 regulates either transporter. Direct evidence would require measurements of transporter activity, phosphorylation state, membrane expression, or other biochemical indices of transporter regulation. I therefore recommend that the authors both temper the mechanistic language throughout the manuscript and explicitly acknowledge in the Discussion that the proposed regulation of KCC2 and NKCC1 is inferred from indirect evidence rather than directly demonstrated in the present study.

(2) The conclusions drawn from the siRNA-mediated knockdown experiments should be interpreted more cautiously. First, it is unclear whether silencing NKCC1 or KCC2 induced compensatory changes in the expression or function of the complementary cotransporter. Given the well-established interplay between NKCC1 and KCC2 in regulating intracellular chloride homeostasis, compensatory adaptations could influence the interpretation of these experiments and should be addressed or acknowledged as a limitation. Second, the sample size for the siRNA experiments appears relatively small. It is unclear how many independent animals contributed slices to each experimental group, making it difficult to assess the degree

of biological replication. In addition, effect sizes are not reported. Clarifying the number of biological replicates and reporting effect sizes would improve the rigor of the statistical analysis and increase confidence in these findings.

(3) The final pharmacological experiments require clarification, as the conclusions appear internally inconsistent. Earlier experiments suggest that the anticonvulsant effects of WNK463 depend on coordinated regulation of both NKCC1 and KCC2. However, in the final experiment, the authors state that simultaneous pharmacological inhibition of NKCC1 and KCC2 does not prevent the anticonvulsant effects of WNK463. In contrast, the accompanying statistical analysis indicates that combined transporter inhibition significantly reduces the effect of WNK463 relative to control conditions. These interpretations appear inconsistent and make it difficult to determine the extent to which the anticonvulsant action of WNK463 depends on NKCC1 and KCC2. The authors should clarify whether simultaneous inhibition of both transporters completely abolishes, partially attenuates, or merely reduces the magnitude of the WNK463 response, and revise the text accordingly. If the effect is only partially attenuated, alternative mechanisms contributing to the anticonvulsant actions of WNK463 should also be considered and discussed.

(4) The statistical analysis and reporting require further attention. First, median values should not be reported with standard deviations, as standard deviation describes variability around the mean rather than the median. For non-normally distributed data, the authors should report median values together with an appropriate measure of variability, such as the interquartile range (25th-75th percentile) or another suitable summary. Second, in several instances, ANOVA results are reported using only a single degree of freedom value (e.g., page 6, DF = 53). This is incomplete, as an F statistic is defined by two degrees of freedom: the numerator degrees of freedom (between-group variability) and the denominator degrees of freedom (within-group variability). Reporting statistical results using standard notation (F(df_between, df_within) = F statistic, p = value) would improve clarity and allow proper interpretation of the analyses.

https://doi.org/10.7554/eLife.112181.1.sa0